Heat Transfer and Latent Heat Storage in Inorganic Molten Salts for Concentrating Solar Power Plants

Final Report

Report Number: DOE-GO18148

Phase I & 2

Prepared by

Anoop Mathur (Terrafore Inc.)
Rajan Kasetty (Terrafore Inc.)
Prof. Javier Garay (UCR)
Prof. Chris Dames (UCR)
Corey Hardin (UCR)
Mehrnoush Zare (UCR)
Mike McDowell (PWR)
Gyan Hajela (PWR)
Dr. Subbarao Surampudi (JPL)
Dr. Andrew Kindler (JPL)
Dr. Parthasarathy Shakkottai (JPL)
Dr. H. Venkatasetty (Setty Enterprises)

May 14, 2012

Submitted to
U.S. Department Of Energy
Contract: DE-FG36-08GO18148

Contact:
Anoop Mathur
Terrafore, Inc.
100 South 5th St, Suite 1900, Minneapolis, MN 55402
anoop.mathur@terrafore.com

.

Table of Contents

Section 1
Project Executive Summary

Motivation for Research

A major issue preventing the commercial use of Phase Change Material (PCM)-based Thermal Energy Storage (TES) is the difficulty of discharging the latent heat stored in the PCM melt. This is because when heat is extracted, the melt solidifies onto heat exchanger surface decreasing the heat transfer. Thus, to obtain consistently high heat rates salt must be removed continuously from heat exchanger surface to improve the heat transfer coefficient and reduce heat exchanger size to obtain the required high and on-demand heat rates in a solar power plant.

Proposed Technical Innovation

Our innovative approach to solve this problem is to use inorganic salt mixtures that have a *simple* phase diagram and a mixture with a *dilute eutectic* composition[1]. A property of dilute eutectic is that when it freezes, it has an equilibrium liquid associated with it. This solid with the associated liquid has the consistency of *a slurry*, which can be pumped to an external heat exchanger, thus forcing the molten salt over the heat exchanger tubes and causing the freezing solid particles to remain in the molten slurry. The forced convection heat transfer due to flow velocity is significantly larger than conduction through solid. In addition to this, a 'salt-phobic' coating on the heat exchanger surface can further prevent the salt from sticking to the tubes and a nucleating agent and chemical added to the salt mixture that can help with the flow and heat transfer properties.

Objective & Technical Approach

A few of the key tasks conducted for this research included:

- Identify economical salt mixtures for use with CSP plants – Power Towers, Linear Fresnel Reflectors and Parabolic Troughs
- Experiment with several different salt-phobic coating candidates
- Understand the morphology of the freezing dilute eutectic salt consisting of 98% NaNO3 and 2% NaOH. Other salt compositions were studied as well.
- TerrDesign a laboratory scale flow loop experiment using a heat exchanger with coated-tubes with salt flowing on the coated tube side and a coolant inside the tubes.
- Demonstrate
    - Improved heat transfer by using a special salt mixture composition called *dilute eutectic* and by coating heat transfer tubes with material that inhibits sticking.
    - A freezing slurry of salt can be pumped over coated tubes without the salt sticking to the tubes. The goal is to freeze 30% to 40% PCM.

[1] Concept of simple phase diagram and dilute eutectic is explained in Section 3

Expected Benefits

The following benefits are expected from using PCM TES, if at least 40% solidification can be achieved with proposed active heat exchanger concept:

- About 20% reduction in amount of salt and 50% reduction in container size compared to equivalent two-tank sensible heat TES.
- Improved overall CSP system efficiency by 1% to 2%
- Reduced TES costs by 30% over conventional two- tank sensible heat TES resulting in a potential reduction in life cycle cost of electricity (LCOE) costs by about 6%.

Accomplishments

The accomplishments for Phase 1 and Phase 2 projects conducted during 2009, 2010 and 2011, included the following:

- Selected salt mixtures suitable for commonly used steam cycles (6 MPa to 13 MPa steam pressures and steam temperatures to 560 degree Celcius) with various CSP plants
- Identified and characterized two candidate coating technologies for use with heat exchanger.
- Developed an experiment setup for qualifying coatings as 'anti-stick' to selected salt mixture. In the experiment rig the salt mixture is pumped through an external heat exchanger with partial frozen salt slurry returning to tank.
- Developed a mathematical model of the PCM storage system and integrated with power tower CSP plant simulation model
- Designed a shell and heat exchanger with coated tubes and integrated it with molten salt flow loop experiment setup. The laboratory prototype used 12000 lbs of dilute eutectic NaNO3-NaOH salt mixture with a storage capacity of about 150 kWh(t) to deliver heat rate up to 30 kWt
- Demonstrated 15% solidification with actively pumping freezing salt over the coated heat exchanger tubes.
- Conducted tests by pumping salt over a coated heat exchanger and collected data to quantify heat transfer coefficient. The results compared well with the model.
- Estimated heat transfer coefficient of 600 W/m2-K with active pumping of freezing salt.

Key Findings

- Dilute eutectic (hyper-eutectic) mixtures of inorganic salts that form a simple eutectic phase diagram exhibit slurry like properties. This property can be taken advantage of to pump salt mixtures over coated heat exchanger tubes and improve heat transfer when PCM is used for storing thermal energy
- Successfully pumped a dilute eutectic molten salt mixture near its freezing point over the specially coated heat exchanger tubes and achieved partial solidification demonstrating use of latent heat of fusion while increasing the heat transfer coefficient. The heat transfer coefficient increased by ten-fold over a passive PCM-TES. However, the solidification achieved was only 15% which is lower than the project milestone of 40%.
- Simulations show that the PCM-TES system can improve the overall system efficiency of the CSP plant by 0.8%, thus requiring about 8% less storage for same capacity factor. This is because for a short period of time, the receiver can be operated to collect energy at lower

temperature to melt the salt, which reduces radiation losses from the solar receiver and increases the collection efficiency. This in turn also allows useful energy to be collected during periods of low insolation by running the receiver at lower temperatures.

- With the use of only 15% latent heat in PCM salt, the net specific cost of PCM-TES using the active heat exchanger described in this document is projected to be only 9% when compared to a two-tank conventional sensible storage system. If credit is taken for the improvement in the overall system efficiency, then these savings increase to 17%. The project goal for cost reduction was 30%.
- Even though, these savings are after paying for the added cost of coated tube heat exchanger, there is uncertainty in our estimate of the cost of the parasitic energy for pumping. In addition, since we are pumping molten salt at freezing point, we expect significant issues with designing and operating with heat tracing system to prevent freezing inside piping. Any incident with freeze-up during operation will reduce the savings.
- Significant lessons were learnt when pumping salt mixtures near freezing temperatures through pipe fittings, valves, bends, and pumps. Heat tracing, location and prevention of solidification and high pressures in unwanted areas require special engineering design and care. The failure mode effect analysis, the experienced gained and the designs developed can be used for any sensible or latent heat system where high temperature molten salt is pumped.

Project Team

US Department of Energy Project Officers – Brian Hunter, Joe Stekli, Tommy Rueckert
Terrafore Inc., MN (Lead)
University of California at Riverside, CA (UCR)
Pratt & Whitney Rocketdyne, CA (PWR)
Jet Propulsion Labs, CA (JPL)
H.V. Setty Enterprises, MN

Report

The report documents the specialty coatings, the composition and morphology of hypereutectic salt mixtures and the results from the experiment conducted with the active heat exchanger along with the lessons learnt during experimentation.

Section 2
Background and Introduction

A key technological issue facing the success of future Concentrating Solar Thermal Power (CSP) plants is creating an economical Thermal Energy Storage (TES) system. Current TES systems use either sensible heat in fluids such as oil, or molten salts, or use thermal stratification in a dual-media consisting of a solid and a heat-transfer fluid. However, utilizing the heat of fusion in inorganic molten salt mixtures in addition to sensible heat , as in a PCM-based TES, can significantly increase the energy density of storage (by about 45%) requiring less salt and smaller containers.

A major issue that is preventing the commercial use of PCM-based TES is that it is difficult to discharge the latent heat stored in the PCM melt. This is because when heat is extracted, the melt solidifies onto the heat exchanger surface decreasing the heat transfer. Even a few millimeters of thickness of solid material on heat transfer surface results in a large drop in heat transfer due to the low thermal conductivity of solid PCM. Thus, to maintain the desired heat rate, the heat exchange area must be large which increases cost. Another issue is finding low cost salt mixtures with good thermal properties and high heat of fusion.

Our innovative approach to solve this is to use inorganic salt mixtures that have a *simple phase diagram* and the mixture is a *dilute eutectic composition*. These two new terms – *dilute eutectic and simple phase diagram* – are explained later. A property of dilute eutectic is that when it freezes, it has an equilibrium liquid associated with it. This solid with the associated liquid has the consistency of a slurry, which can be pumped to an external heat exchanger, thus forcing the molten salt over the coated heat exchanger tubes and causing the freezing solid particles to remain in the molten slurry. The forced convection heat transfer due to flow velocity is significantly larger than conduction through solid. In addition to this, *a 'salt-phobic' coating* on the heat exchanger surface can cause the salt to adhere to the tubes lightly, so that it can be easily removed by the flowing salt.

Thus, two key considerations for designing a successful PCM storage system would be:

- Selecting a storage media in the approximate temperature range of 275 C to 350 C with the following desired properties :
    - High energy density. This requires less TES material and hence smaller tanks, lower cost, and lower thermal loss during storage.
    - High chemical and thermal cycling stability
    - Complete reversibility for a large number of charge and discharge cycles
    - Low specific cost
    - Readily available and easy to handle with low toxicity and low corrosivity
- Designing a heat exchange mechanism that minimizes the cost of the heat exchanger. To discharge heat from a PCM-based TES, a good heat exchanger should have the following properties:
    - have a high heat transfer coefficient throughout the discharge
    - use low parasitic power for pumping, if using an active heat exchanger
    - use common heat exchanger designs, such as shell and tube, that can be manufactured using state-of-the-art techniques

In the following sections we describe a baseline CSP plant, prior art in designing active heat exchangers for PCM-TES and our approach of a shell and coated tube heat exchanger.

Baseline CSP Plant with PCM-TES

Te

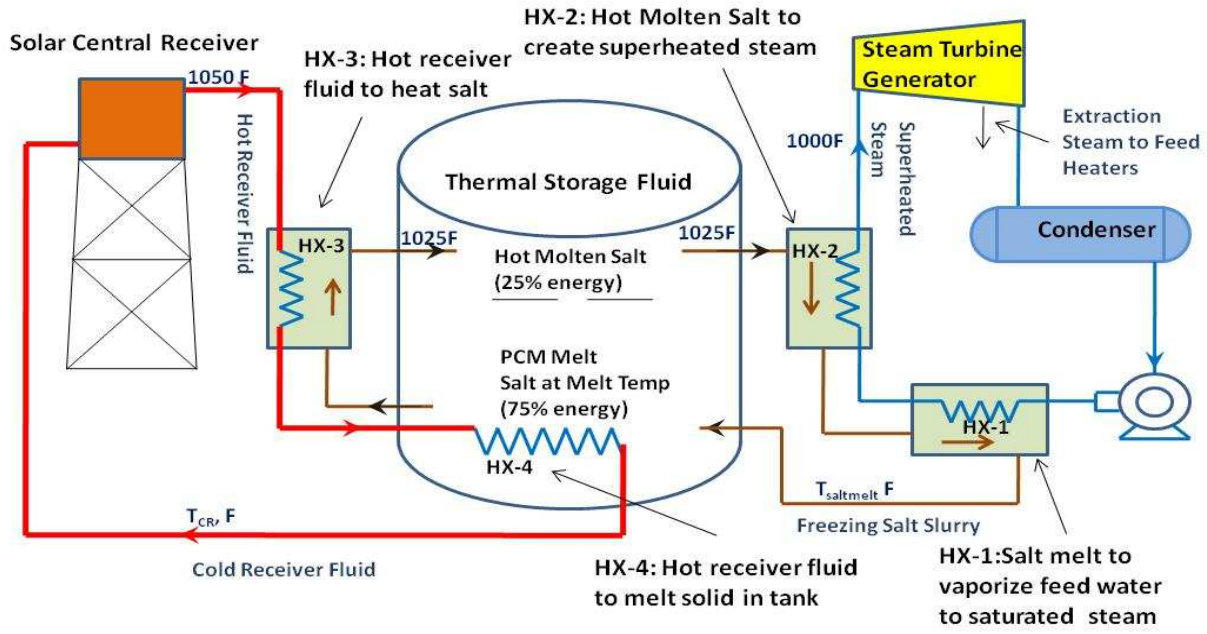

Figure 1.1. PCM-based TES design offers a low cost approach by reducing the TES system size by 37% to 56%

A baseline system using power tower is shown in Figure 1.1. This figure shows a PCM-based TES system with a single tank, in a power-tower configuration. In this configuration, thermal energy is stored as a combination of latent heat and sensible heat in an inorganic molten salt mixture. In the figure, the fluid at the bottom of the tank labeled- *PCM Melt*– stores up to 75% of the total heat at a constant melt temperature of 310^{o}C (590 F) as heat of fusion in an inorganic salt mixture consisting of a large percentage by weight of sodium nitrate and a small amount of sodium hydroxide (this proprietary composition is described later as the *dilute eutectic*). The fluid labeled – *Hot Molten Salt* – stores the remainder 30% of heat as sensible heat in salt temperatures between the melt temperature and up to 565^{o}C (1025 F). The ratio of latent heat stored to sensible heat depends on the latent heat of fusion of selected salt mixture and the high and the low operating temperatures (the low operating temperature is typically the melting point of the salt.)

Starting from the right of the tank in Figure 1, high pressure 8.6 MPa (1250 psia) feed water from the condenser is vaporized into a saturated steam at 300^{o}C in a steam generator heat exchanger *HX*-1. Superheat is added to the saturated steam in the superheat heat exchanger *HX-2*. This superheated steam at 540^{o}C (1000 F) is delivered to the Steam Turbine Generator. The heat for superheating steam and vaporizing feed water is provided by pumping the hot molten salt from top of tank, first to *HX-2* and then to *HX-1* as shown in the figure. The salt is cooled to the freezing or melting point of salt in HX-1 causing some salt to solidify. The partially-frozen salt-slurry from *HX-1* is returned to the tank.

On the left of the tank in Figure 1, the hot receiver fluid from the Solar Central Receiver (power tower) transfers heat to the molten salt in the tank in a heat exchanger labeled *HX-3*. Then the fluid is directed to the heat exchangers labeled *HX-4* to melt the salt in the tank. The cold receiver fluid from *HX-4* is returned to the Solar Central Receiver to collect solar heat. (The return temperature of the cold receiver fluid is at 315^{o}C (600 F) slightly higher than the melt temperature of 310^{o}C . The heat transfer fluid (HTF) in the receiver can be any advanced heat transfer fluid such as another thermally-stable molten salt mixture or liquid sodium or oil.

In state-of-the-art CSP systems which use a two-tank sensible TES, the HTF is same as the storage fluid and since large volumes of this fluid are required, the HTF selected must be economical. However, with PCM-TES shown, an HTF can be chosen independent of the TES storage salt. Since the fluid required to collect energy in the receiver fluid is independent of TES salt, an efficient HTF which can operate at higher temperatures can be selected. For example, if this temperature can be increased to 600^{o}C (1110F), then the hot molten salt temperature in the TES tank can be raised to 580^{o}C (1075F) instead of the 1025F and the steam delivered to turbine can be raised to a higher temperature which will increase the heat to electrical conversion efficiency in the turbine generator.

Designing an Active Heat Exchanger

There are many types of heat exchangers used in the industry for transferring heat during phase change from liquid to solid. Some of the active (not passive) heat exchange designs include shell and coated tubes; others use mechanical scrapers, ultrasonic vibrations or flexing to free the tubes of freezing salts. Other active heat exchanger designs include microencapsulating the salt and pumping it by carrier fluid or by simply having water in direct contact with the molten salt to generate steam. Some of these designs were built and tested for PCM-TES systems in the early 1980s. However, the research was incomplete due to change in US DOE energy focus in 1981.

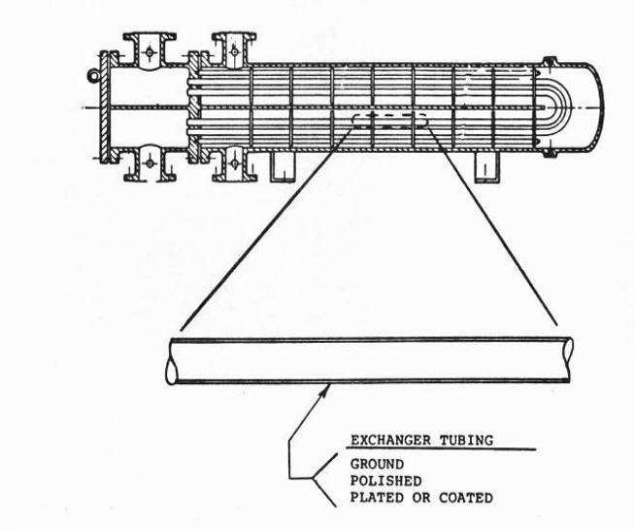

Figure 2.Low adhesion surfaces and shell and tube heat exchangers offer economical design options

Our preliminary analysis and experience, based on this past research, indicated that a shell and tube type of heat exchangers, with the salt on the shell side and the two-phase steam water inside the tube (Figure 1.2), can potentially be successful when discharging heat from the PCM melt. Furthermore, since this is a commonly used design in the industry it is also the most economical to use.

Our baseline approach was to simulate and test various configurations of the shell-and-tube exchanger and by coating the tubes with a material to render it smooth to prevent freezing PCM solids from adhering to it during heat transfer through the tube surface.

Research on Additives and Coatings

A major drawback of using phase change molten salt materials is their poor thermal conductivity and the fact that clumping occurs during freezing that sticks to the walls of the storage tank and heat exchanger surfaces. Using our proposed storage media of dilute eutectic would alleviate this problem. To further improve the flow properties and improve the conductivity, we proposed to investigate use of additives such as graphite, nano-carbonaceous materials, and ionic liquids. Since coatings also alleviate the problem of the phase change materials sticking to the walls, we proposed to investigate heat exchanger coating materials such as graphite, metallic nitrides and carbides, and high temperature polymers (such as imides, poly benzo-oxy imidazole). We propose these materials because of their high thermal stability, and chemical stability, good heat transfer properties and good non-wetting characteristics with molten salts.

Research Tasks

The research conducted over the two years included the following and is discussed in sections listed below:

- Selecting a salt mixture for use with various CSP designs (Section 3)
- Conducting research to select a salt-phobic coating for the selected salt mixture (a dilute eutectic of sodium nitrate and sodium hydroxide) (Section 4)
- Characterizing the morphology of dilute eutectic mixture (Section 5)
- Designing a heat exchanger and PCM-TES laboratory prototype(Section 6)
- Conducting experiments by pumping freezing salt mixture using the heat exchanger (Section 7)
- Model and economic analysis (Section 8)
- Lessons learned from the research (Section 9).

Section 3
Selecting Salt Mixtures for Latent Heat Thermal Energy Storage for Concentrating Solar Power Plant (CSP)

Focus of this Section

This section discusses the selection of salt mixtures for storing thermal energy as latent heat of fusion in mixtures of inorganic salts that melt in the range of 275 ^{o}C to 350 ^{o}C.

This melting temperature range is chosen to match the steam vaporization temperatures that are typically used in power generation cycles using Rankine Turbines. The concentrating solar thermal power (CSTP or CSP) plants are being designed to heat fluid from 400 ^{o}C to 565 ^{o}C to provide heat for vaporizing and superheating steam at steam pressure from 5.9 MPa (850 psia, saturated steam temperature of 274 ^{o}C) to 12.4 Mpa (1800 psia , saturated steam temperature of 327 ^{o}C). The salt melting point should be a little higher than the selected saturated steam temperature. Future systems can go up in steam pressures to 16.5 MPa (2400 psia, 350 ^{o}C saturated steam temperature) or even supercritical range (>22.1MPa or >3207 psia).

Melting Point of Salts Required for CSP

The melting point of salt should be higher than the vaporization temperature of steam at the selected steam conditions for the Rankine power cycle. The temperature difference is determined by the optimum approach temperature for heat transfer from freezing salt to boil steam. Typically this is between 15 C to 25 C depending on the cost of the coated tube boiler (heat exchanger).

The following Table 2.1 gives the required melting points of salts for Concentrating Solar Thermal Power (CSP) systems which include: Solar Central Receiver (Power Tower), Parabolic Trough, and Linear Fresnel Reflectors. For utility scale power generation generating electrical power between 50 MW(e) to 100 MW(e), these use Rankine steam turbines. The steam pressures and temperatures to these turbine range from 5.9 MPa to 22.1 MPa with superheated steam of 400 ^{o}C to 565 ^{o}C. Table 1 shows the typical steam conditions for the various CSP technologies. A large of the heat is required to vaporize steam at constant saturated steam temperature shown in the table. Thus for generating power through storage, a large fraction of heat must be stored above the saturation steam temperatures (for example at 8.6 MPa and 565 ^{o}C turbine conditions, the heat of vaporization at 300 ^{o}C is 70% and the sensible heat between saturated temperature of 300C and superheated temperature of 565 ^{o}C is 30%). The desired salt melting temperature should be 5 C to 10 C higher than the saturated steam temperature, as shown in Table-1. Next generation power tower systems are expected to use supercritical pressures of 22.1 MPa. The higher pressure steam turbine cycles are more efficient and will significantly improve the overall plant efficiency and hence the economics. Therefore, in this report we considered salts for steam cycles up to 16.5 MPa.

Table 1 Salt Melting Temperatures Required for Various Power Plant Cycles

CSP Technology vs. Steam Conditions	Next generation Power Tower CSP Next generation Troughs & Fresnel CSP SOA Power Tower CSP SOA Fresnel CSP SOA Parabolic Trough CSP					
Steam Pressure, MPa (psia)	5.9 (850)	8.6 (1250)	10.0 (1450)	12.4 (1800)	16.5 (2400)	22.1 (3200)
Saturated Steam Temperature, deg C (deg F)	274 (527)	300 (572)	311 (599)	327 (617)	350 (662)	373 (705)
Desired Salt Melting Point, deg C (deg F)	285 (545)	310 (590)	320 (608)	340 (644)	360 (680)	400 (752)

Concept of *Simple Phase Diagram and Dilute Eutectic*

In a *dilute eutectic* mixture 96% to 98% by weight is of the major component of the salt mixture and remainder is a selected minor component salt mixture. The salts in Table 3 can be used as a major component in combination with a salt that can form a eutectic with a minor component (2% to 4% of the mixture weight). For example, there are 29 different salt systems with NaOH, 123 salt systems with KNO3, 117 salt systems with NaNO3 and so on. Our approach requires us to select the minor component that forms a *simple phase diagram* or no solid solutions as the mixture solidifies. This is because we require the solid that crystallizes out during solidification should be in equilibrium with a liquid. In the phase diagram, shown in Figure 3 and discussed below this is the region between the melting point of major component and the eutectic point of the mixture.

An example of a simple phase diagram and dilute eutectic composition is described below using a NaNO3-NaOH system.

Figure 1 shows a *simple phase diagram* of a NaNO3-NaOH system. In a *simple phase diagram* there are no solid solutions as is shown on the right or the NaNO3 side of the figure. The eutectic composition is 83.2% NaNO3 and 16.8% NaOH and eutectic temperature is 246 ^{o}C. The selected composition of 97% NaNO3 and 3% NaOH for TES has much larger percentage of NaNO3 than the eutectic composition and hence the term *dilute eutectic composition* in NaNO3. The storage temperature at the start of a discharge cycle is closer to the melting point of NaNO3 which is 310 ^{o}C. As heat is extracted, only NaNO3 component crystallizes out (since there are no solid solutions on this side) leaving an equilibrium liquid composition along the liquidus curve.

For example, for the selected dilute eutectic after 50% of the NaNO3 freezes out, the equilibrium liquid will contain 47 units of NaNO3 and the original 3 unit of NaOH. This calculates to a liquidus of 94%

NaNO3 and 6% of NaOH. From the curve we can see that the freezing temperature for 94% NaNO3 and 6% NaOH is 305 ^{o}C. Thus, after 50% of heat is removed from the melt, the temperature only drops from the initial 310 ^{o}C to 305 ^{o}C, which is not a significant drop in temperature while the latent heat is stored at near constant temperature. This is the reason to use a dilute eutectic as a starting mixture. We must ensure that the heat exchanger tube temperature is kept above the eutectic temperature of 246 ^{o}C so that the solid on the tubes has a liquid in equilibrium with it. To ensure this we require that the salt system should not have any solid solutions between its initial melting temperature and eutectic point.

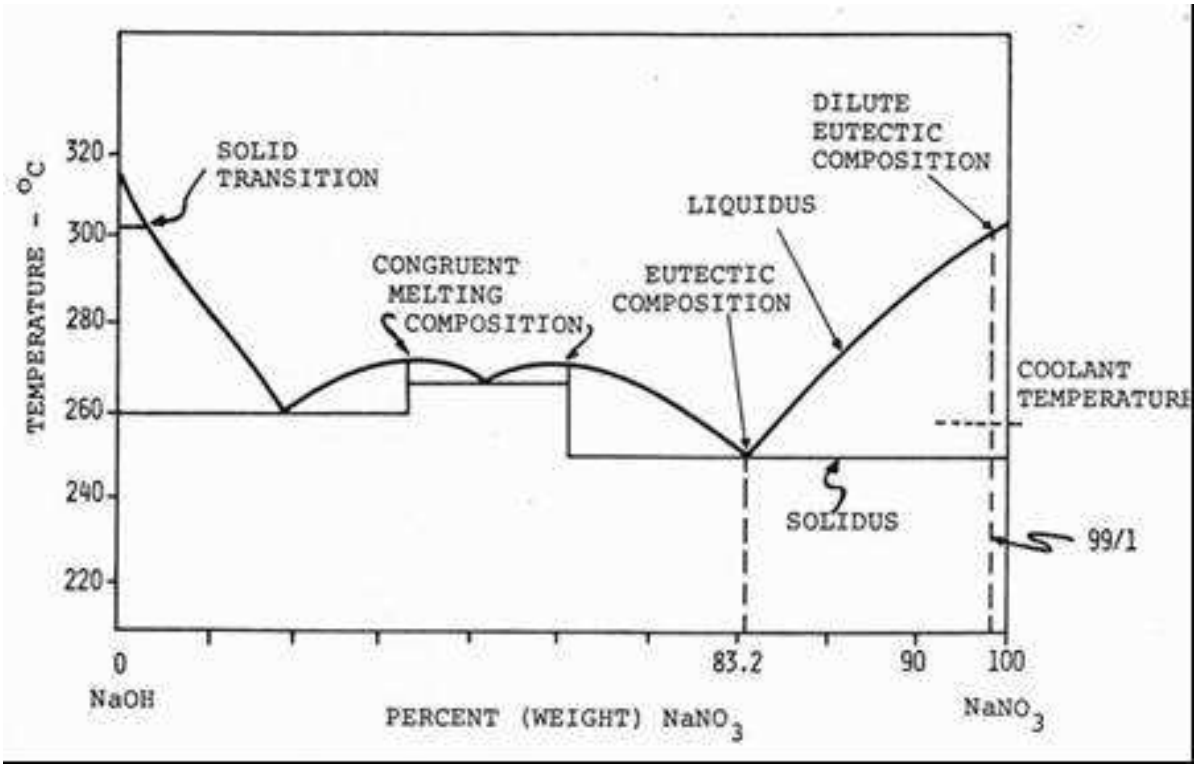

Figure 1: Phase Diagram of NaNO3-NaOH system

There are numerous salts and salt mixtures that have melting points within the range of the CSP application. In addition to melting point and low cost per unit weight the selected salt must have several desirable properties. Figure 2.1 shows a process for selecting salts.

Ideally the selected salt must:

- be easily available
  be thermally stable and withstand multiple freeze-thaw (>5000) cycles
- have high specific heat of fusion (kJ per kg and kJ per m^3),
- should be less corrosive to commonly used containers (eg, steels). Since the salts will be of commercial grade, the levels of impurities, particularly such as chloride and moisture are important as they affect corrosion to container materials
- have a low vapor pressure at temperature (up to 550 ^{o}C),
- be non-hygroscopic, reactive or non-toxic so it can be handled and stored easily,
- has good thermal properties such as thermal conductivity.

Most salts are hygroscopic and in addition to impurities, moisture should be avoided as they affect the corrosion properties as well as heat of fusion of salts (3). During thermal cycling process, there will be interactions between the molten eutectic mixture and the surface of the container, and the resulting impurity is likely to increase and however small amount it may be, compared to the eutectic mixture, and likely to affect the rate of nucleation and crystallization during phase-change.

Appendix 2.1 lists all the salt mixtures that have been studied and have melting points within the range of 275 ^{o}C to 375 ^{o}C. We first screen salt mixtures from the list in Appendix A by using the criteria in Table 2 which is a qualitative evaluation of inorganic salt mixtures by category. In the Terrafore concept for thermal storage, the salt mixture is a 'dilute eutectic' salt mixture consisting of a major component (which is typically much greater than the composition at the eutectic) in the salt mixture and a minor component, which is the remainder. The 'yes' in Table 2.2 indicates the salt is acceptable and 'no' indicates it is not acceptable. Some salts which may not be acceptable as major component may qualify for use as a minor component.

Based on this, salts containing chlorides, nitrates and hydroxides may be selected as a major component. Next, salts that contain exotic or uncommon metals are rejected. For example, salts containing noble metals such gold, silver, platinum, tungsten, cadmium etc are expensive, and are not readily available in very large quantities. These are not selected even as minor components. Since Lithium salts have very high heat of fusion, we kept this in the short list in Table 2.3, which lists the major component of the salt mixture suitable for CSP applications. This (Table 3) is a short list of thirty one salts and salt mixtures that have melting points within the 275 ^{o}C to 375 ^{o}C range, have many desired properties such as thermal stability and availability for use in TES applications. The rightmost column in the table shows the steam cycle for which the salt can be used. Salts such as NaNO3, NaOH, KNO3 and KOH are highlighted as selected major component. Next we use the simple phase diagram criteria (discussed later) with any of these four major components. When alternative salt mixtures that have simple eutectic diagram are available within the steam cycle, we reject salt mixtures that contain component(s) that are either corrosive or are expensive. For example, the fluorides or the chromate or zinc chloride in the Table 2.2 even in small quantities can be problematic. If there is an alternative to any of these we select that salt mixture as the major component

Table 2. Various categories of salts and their characteristics

Salt Category	Qualitative Characteristic of Salt	Major Component	Minor Component
Chlorides	Low cost, good thermal properties, readily available in large quantities. Corrosion is an issue and must be addressed (*)	Yes	Yes
Hydroxides	same as above	Yes (?)	Yes
Nitrates	same as above	Yes	Yes
Nitrites	same as above but oxidizes easily, low vapor pressure, not very stable	No	Maybe
Carbonates	applicable temperature range high; good additives	No	Yes
Sulfates	Corrosive	No	Yes
Oxides	Corrosive	No	No
Fluorides	Fluorides not available in large quantities. Most Flouride salts that melt below desired temperature range contain expensive Li or alkali metal	No	Yes

(*) Chlorides, sulfates, phosphates are present in smaller quantities in most salts obtained in bulk and corrosion has to be addressed in selecting any salt mixture.

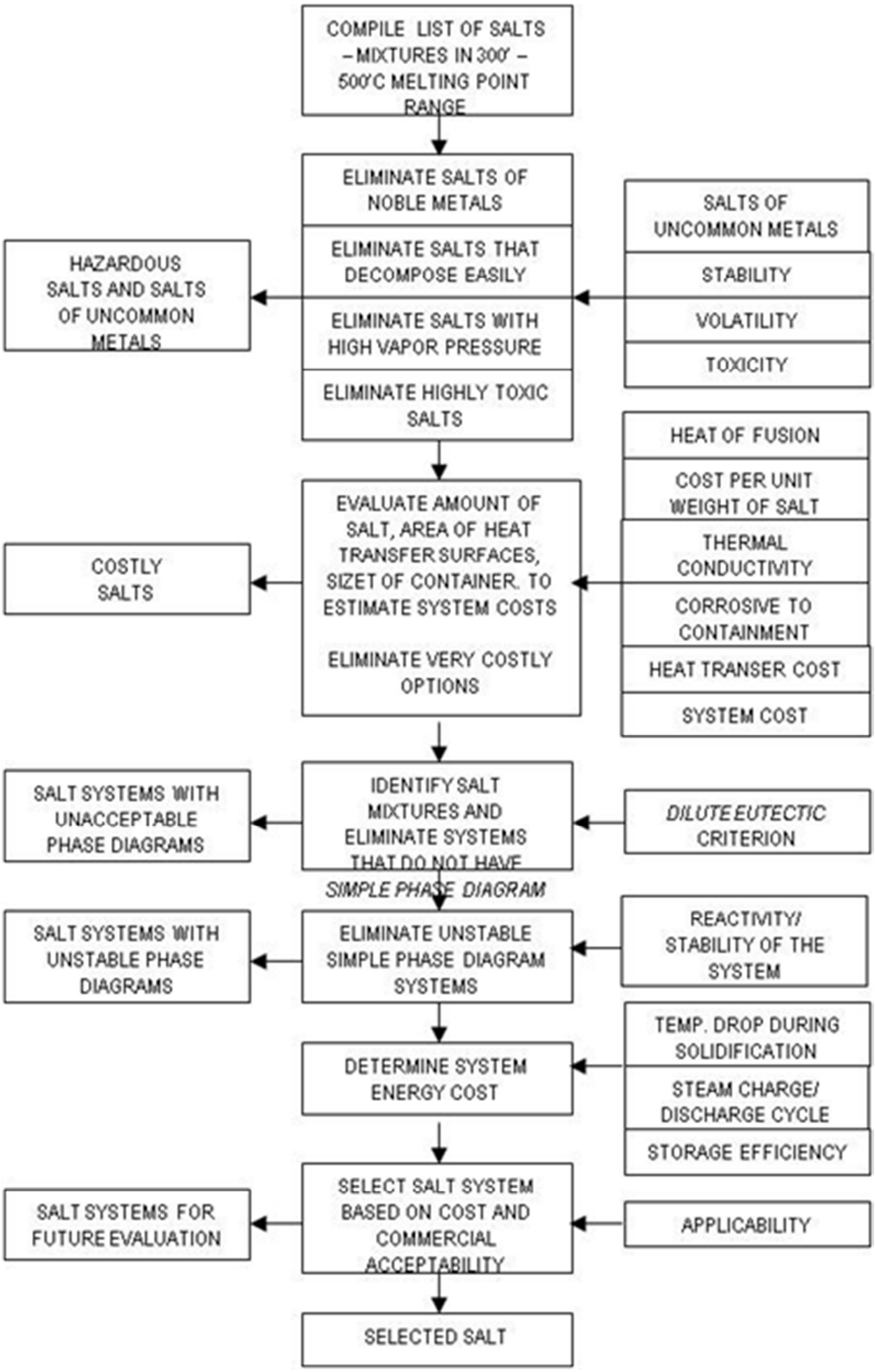

Figure 2. Method for Selecting Salt Mixtures for CSP Application

Table 3. Candidate Salt & Salt Mixtures for use with CSP- TES as a Major Component

	System	Eutectic Temp, deg C	Composition (mole percent)	Formula Wt	kJ/kg	Steam Cycle
1	NaNO3-NaCl-Na2SO4	278 C	86.3-8.4-5.3	85.79	190.22	1
2	LiCl-LiOH-KCl	280 C	45-43.5-11.5	27.66	763.33	1
3	NaNO3-NaCl-Ba(NO3)2	280 C	86.2 -7.9-5.8	93.02	175.90	1
4	NaNO3-NaCl	281 C	98.9-1.1	84.71	175.59	1
5	NaOH-NaCl-Na2CO3	282 C	85.8-7.8-6.4	45.66	206.62	1
6	ZnCl2 (**)	283 C	100	136.00	75.37	1
7	NaOH-Na2CO3	283 C	92.8-7.2	45.42	199.95	1
8	NaOH-NaCl-Na2CO3	291 C	87.3-6-6.6	45.42	199.95	1
9	NaNO3-NaBr (**)	293 C	90.5-9.5	86.71	182.32	1
10	NaOH-Na2SO4	293 C	95.3-4.7	44.79	160.19	1
11	NaNO3-Ba(NO3)2 (**)	294 C	93.6-6.4	96.26	159.89	1
12	KCl-ZnSO4 (**)	295 C	66.6-33.4	103.46	203.86	1
13	NaNO3-NaCl	297 C	93.5-6.5	83.27	187.22	1
14	KNO3-KF	298 C	91-9	97.13	135.93	1
15	NaNO3 - NaCl	298 C	95-5	83.67	183.95	1
16	NaNO3-Na2SO4	300 C	95.5-4.5	87.57	172.81	1
17	NaNO3-NaF	304 C	96.5-3.5	83.50	184.30	1
18	NaNO3	310 C	100	85.00	173.27	1,2
19	NaOH - NaCl	314 C	93.7 -6.3	41.16	187.62	2
20	NaOH	318 C	100	40.00	158.99	2,3
	Salt System	Deg C	Mole%	Formula Wt	kJ/kg	Cycle

21	KNO3-Ca(NO3)2-K2CRO4 (**)	319 C	99.18-0.12-0.70	100.37	118.59	2,3
22	KNO3 - KCl	320 C	94-6	99.42	126.78	2,3
23	Na2CO3-Na2SO4	330 C	66.5-33.5	56.00	474.81	3
24	KNO3-K2SO4	334 C	98.8-1.2	99.79	120.55	3
25	KNO3 – KBr (**)	336 C	99-1	101.18	117.15	3
26	KNO3	337 C	100	101.00	115.99	3
27	LiCl-KCl-LiF	346 C	56-40.5-3.5	56.16	408.93	4
28	LiCl-KCl-NaCl	346 C	55-36-9	55.43	415.33	4
29	LiCl-KCl	348 C	58-42	55.92	405.77	4
30	LiOH-K2CO3-Li2CO3	350 C	59.1-28.2-12.7	48.31	534.76	4
31	KOH	360 C	100	56.00	167.36	5
Notes	Steam Cycle: 1=5.9 MPa, 2=8.8 MPa, 3=10.0 MPa, 4= 12.4 MPa, 5=16.5 MPa ** Avoid if alternate salts are available. Bromides and chromates are toxic and for large scale systems cannot be used even in small quantities. Lithium salts are included because of their high heat of fusion. Lithium salts are expensive and hygroscopic and require special handling. LiNO3 is perhaps the only exception that may be used in small quantities. Thus from practical standpoint there are very few salts that qualify for use as PCM for TES application.					

Recommended Salts for CSP Applications

We studied phase diagrams for several mixtures with the salts listed in Table 3 and used a combination of criteria discussed earlier (see Figure 2) in the salt selection method such as the simple phase diagram, low cost, low corrosivity, high heat fusion, availability, and experience. Based on this, we selected the salts listed in Table 5 as recommended salt mixtures for the different steam cycles. The percentage by weight of the major component is much higher than that of the composition of this component at the eutectic point. In case of three salt mixtures, the minor component may be a eutectic of two components and the major component is the third salt. Alternatively, the major component may be a eutectic of two components (example, NaNO3-NaCl in the table) and the minor is the third component.

Nitrate salts have been used extensively in the industry and are readily available in large quantities. Stainless steel is preferred as containment material. Even though mild steel can be used, the incremental cost of stainless steel over mild steel relative to the overall cost of system is small and stainless steel has better corrosion resistance to most salts and impurities. The impurities alter the system properties and the

corrosion properties of the mixture. An assay and thorough analysis of the effect of these impurities is required before specifying and procuring salt mixtures.

For experiments in Phase 2 and Phase 3 of the program we selected a *dilute eutectic* mixture of NaNO3 as the major component and NaOH as the minor component.

Table 4. Selected Salts for Typical Steam Power Plant Cycles

Major Component (Initial Melting Point)	Minor Component	Steam Pressure for CSP / Rankine cycle
NaNO3-NaCl eutectic (294 C)	NaOH	5.9 MPa
NaNO3 (310 C)	NaOH	8.8 MPa
NaOH (318 C)	NaNO3	10 MPa
KNO3 (337 C)	KOH	12.4 MPa
KOH (360 C)	KNO3	16.5 MPa

Section 4
Characterization of Anti-stick Coating using Differential Scanning Calorimeter

Differential scanning calorimeter (DSC) measurements were used to examine the effects of 1)composition, 2) surface roughness, and 3) coating layer, on the solidification temperature of the salts. The cooling rate was also varied (10, 50, 100^{o}C/min). A TA instruments DSC was used in this study.

Effects of salt composition

In order to examine the dependence of the melting and solidification events on of salt composition, different compositions of salt (NaOH/NaNO3) ratios were weighed and mixed for DSC analysis. The salts were transferred to as-received stainless steel DSC pans. In the course of our experiments, the solid salts were heated from room temperature to 350°C and subsequently cooled and repeated; each run comprised 10 different heating-cooling cycles. Figure 1 has the DSC results showing the heat flow vs. temperature for varying compositions of salt. The downward trend of the curve corresponds to the salt melting and the upward trend (peak) corresponds to the solidification event. The results demonstrate that both the melting and solidification temperatures are composition dependent. We also see that for some compositions the curves (different heating-cooling cycles) do not overlap. This is an indication of the lack of repeatability of the melting/cooling. The only composition for which the curves overlap is the 100% NaNO3 sample.

We attribute the lack of repeatability of the samples containing NaOH to corrosion of the stainless steel by NaOH. Corrosion changes the SS surface and also the global composition of the salts and thus the solidification/melting temperatures. These findings show that identifying a coating that minimizes corrosion is crucial.

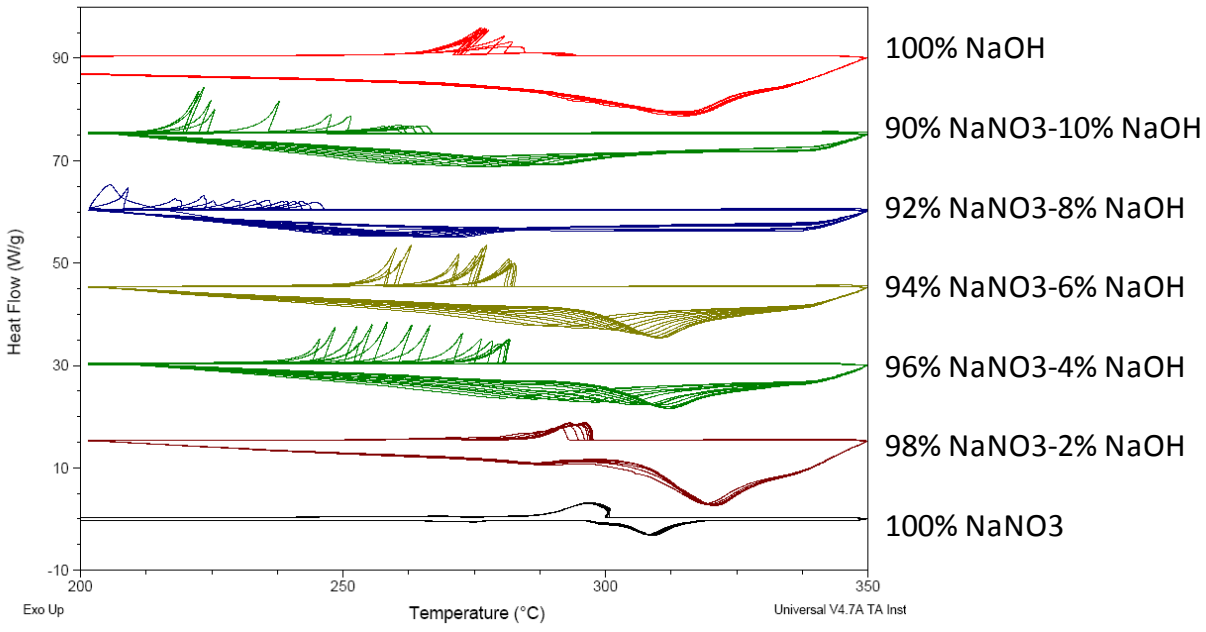

Effects of surface roughness

In order to examine the effects of surface roughness on the solidification event, we systematically varied the surface roughness of the DSC pans by electro-polishing. Figure 2 a and 2 b are pictures of the surface of DSC pans before and after polishing.

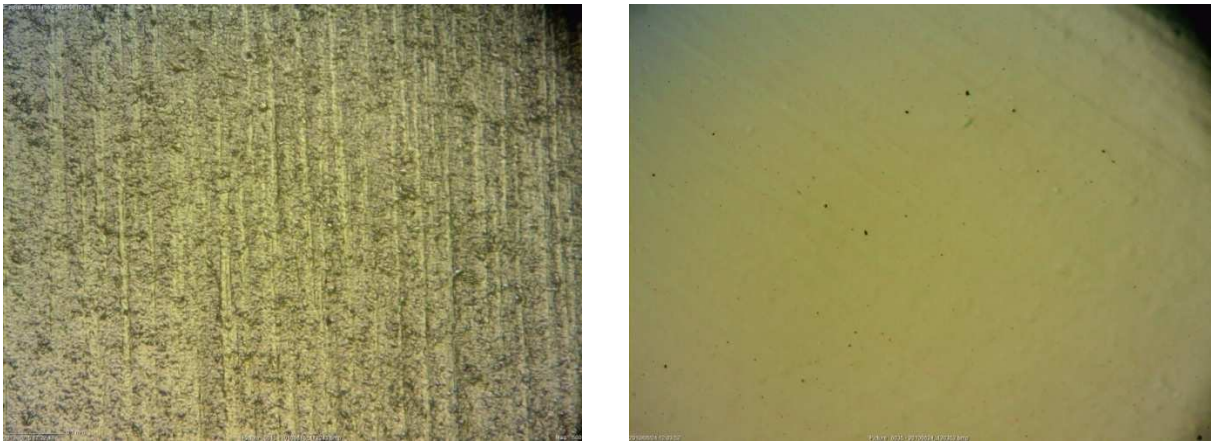

Fig. 2 a) Optical microscope picture of DSC pan before a) and after b) electro-polishing

DSC heating/cooling runs were conducted using DSC pans with various surface roughness using pure NaNO3. Figures 3,4,5 show the results of the tests for varying root means square (RMS) surface roughness with a cooling rate of 10, 50 and 100°C/min respectively.

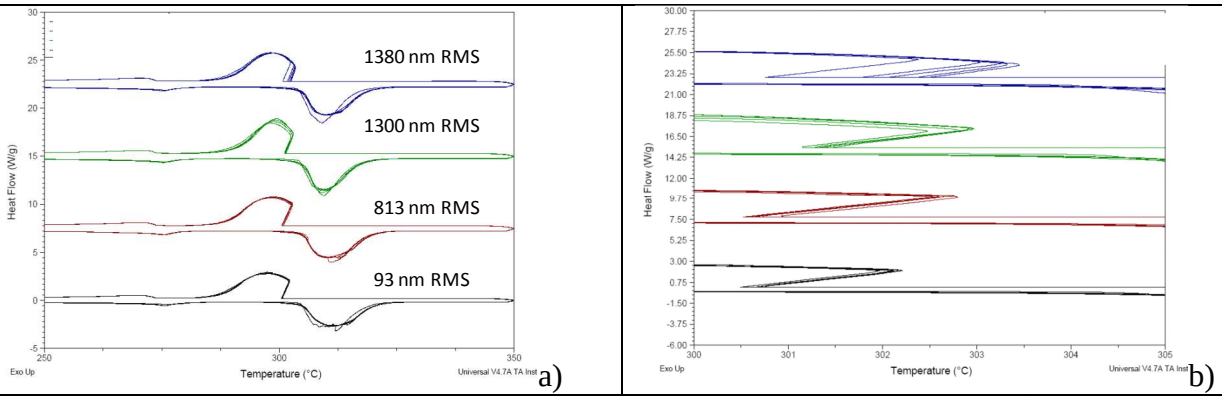

Fig. 3 DSC results for NaNO3 samples with varying surface roughness using 10 ^{o}C/min cooling rate. a) entire temperature range b) narrow temperature range emphasizing solidification event.

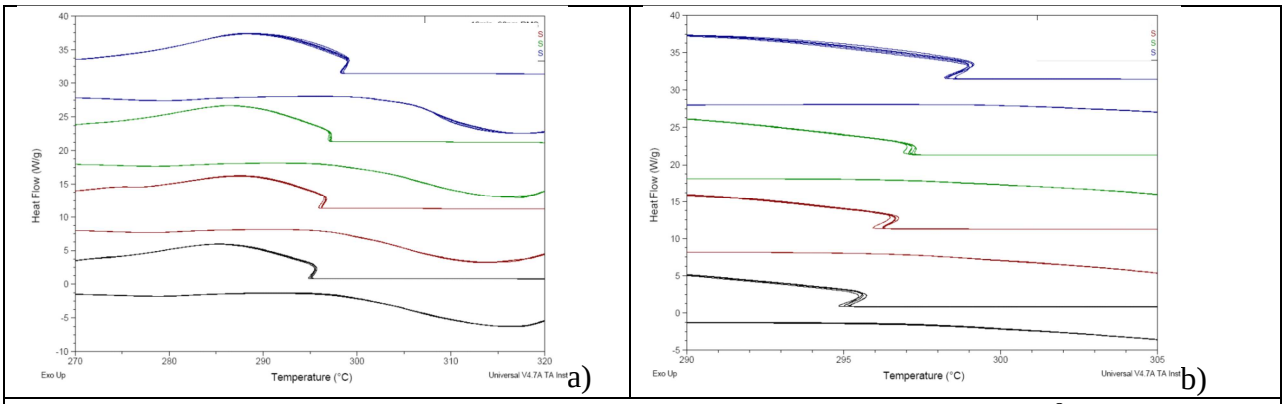

Fig. 4 DSC results for NaNO3 samples with varying surface roughness using 50 ^{o}C/min cooling rate. a) entire temperature range b) narrow temperature range emphasizing solidification event

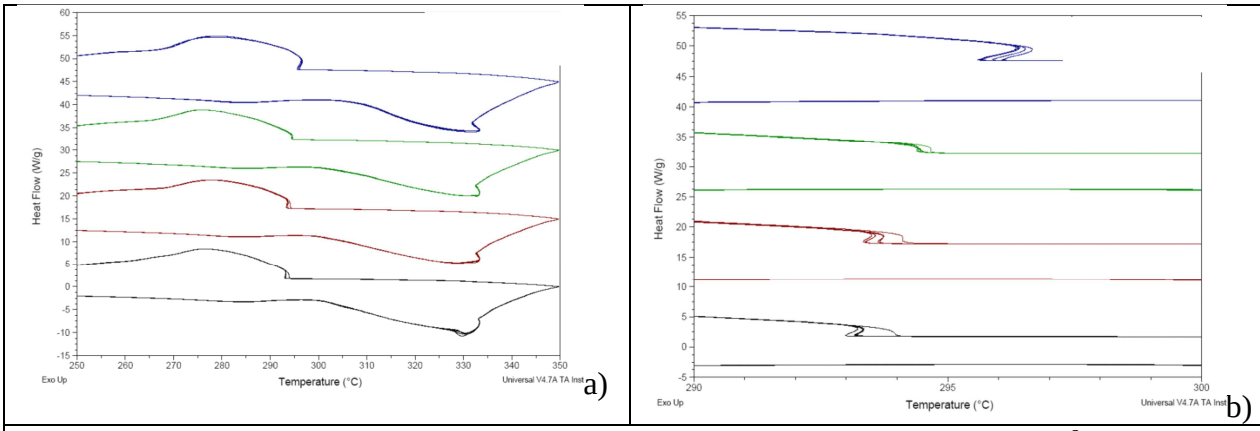

Fig. 5 DSC results for NaNO3 samples with varying surface roughness using 100 ^{o}C/min cooling rate. a) entire temperature range b) narrow temperature range emphasizing solidification event

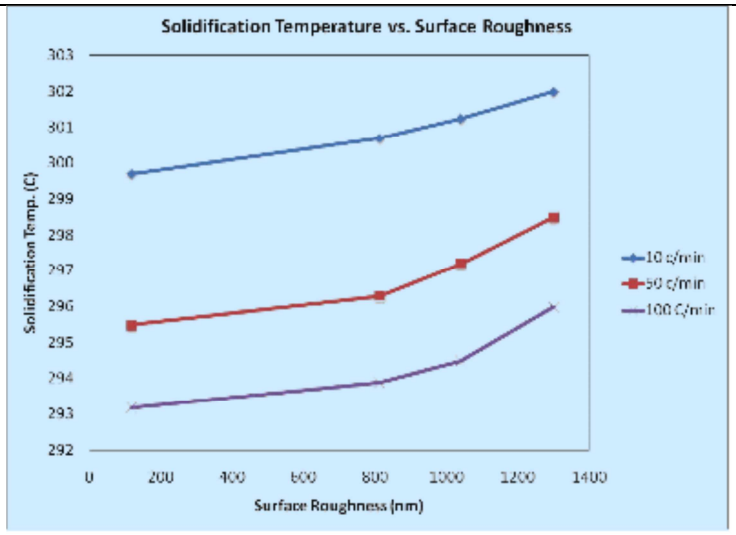

Figure 6 Effect of surface roughness on Solidification temperature for 3 different heating rates.

The results show that decreased surface roughness causes a significant shift of solidification toward lower temperatures for all of the heating rates. The shift is more pronounced at higher heating rates. The shift caused by surface roughness is more appreciable in Figure 6.

Effects of surface composition (coating material)

In order to examine the effects of surface coating on the solidification event, we coated the DSC pan with different materials: Cu, Ag, Ni, Cr, and TiN. Figure 7 are the results of the DSC tests.

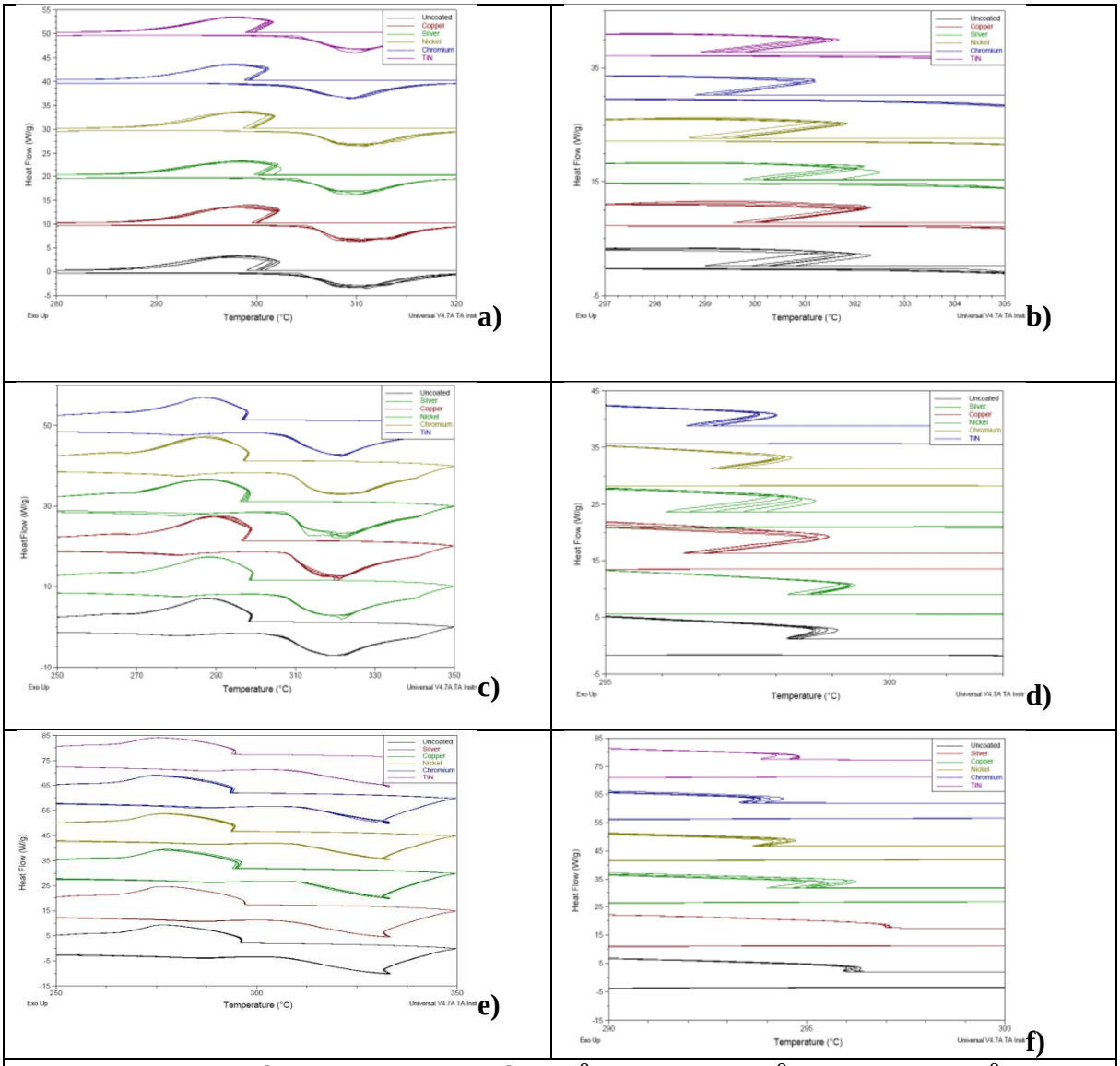

Figure 7 DSC plots for various coatings for 10 ^{o}C/min (a,b), 50 ^{o}C/min (c,d), 100 ^{o}C/min (e,f).

The results show that all of the coating materials cause a shift in the solidification temperature. Ag actually has a negative effect (shifts the solidification temperature to higher temperatures). The rest of the materials decreases the solidification temperature. The shift is largest for the Cr coating.

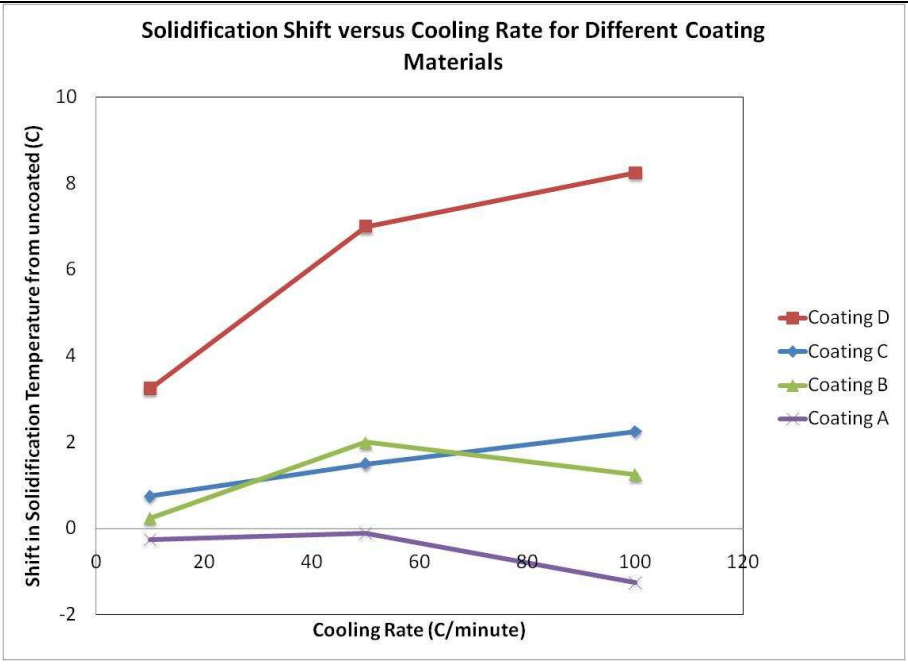

Figure 8 Shift of solidification temperature for different coatings at 3 different cooling rates.

Selected Coating for Experiments with the NaNO3-NaOH Dilute Eutectic Mixture

Seamless heat exchanger tubes were first electropolished and then coated with chromium. The electropolishing solution and method is described in Appendix 2. The morphology of the chrome coating is important.

Section 5
Morphology of Freezing Salt Mixture

According to previous studies, the best binary salt system is NaOH-NaNO3. Fig 1 shows the binary phase diagram for this system. Three different binary compositions were selected for the primary studies in this system. These three compositions are as below:

1- NaNO3 (100%)

2- NaOH (10wt%) – NaNO3 (90wt%)

3- Eutectic composition of: 15.8wt% NaOH-84.2wt%NaNO3

Fig 2 shows the cooling curves for pure sodium nitrate with different amount of purity. In fig 2A, B and C cooling curves are related to sodium nitrate with 98% purity and in all of them transformation temperature is about 300°C with 0.5C accuracy (table 1). Supercooling however varies from 0.1C to 0.4 C. For the 99.999% grade sodium nitrate the freezing point is accurately 308C due to the phase diagram (fig 1). The supercooling however is 0.8C, which is the highest supercooling obtained among all. This can be due to the high purity of NaNO3 and also higher cooling rate. Note that the temperature accuracy is less than 0.07C with the instruments used.

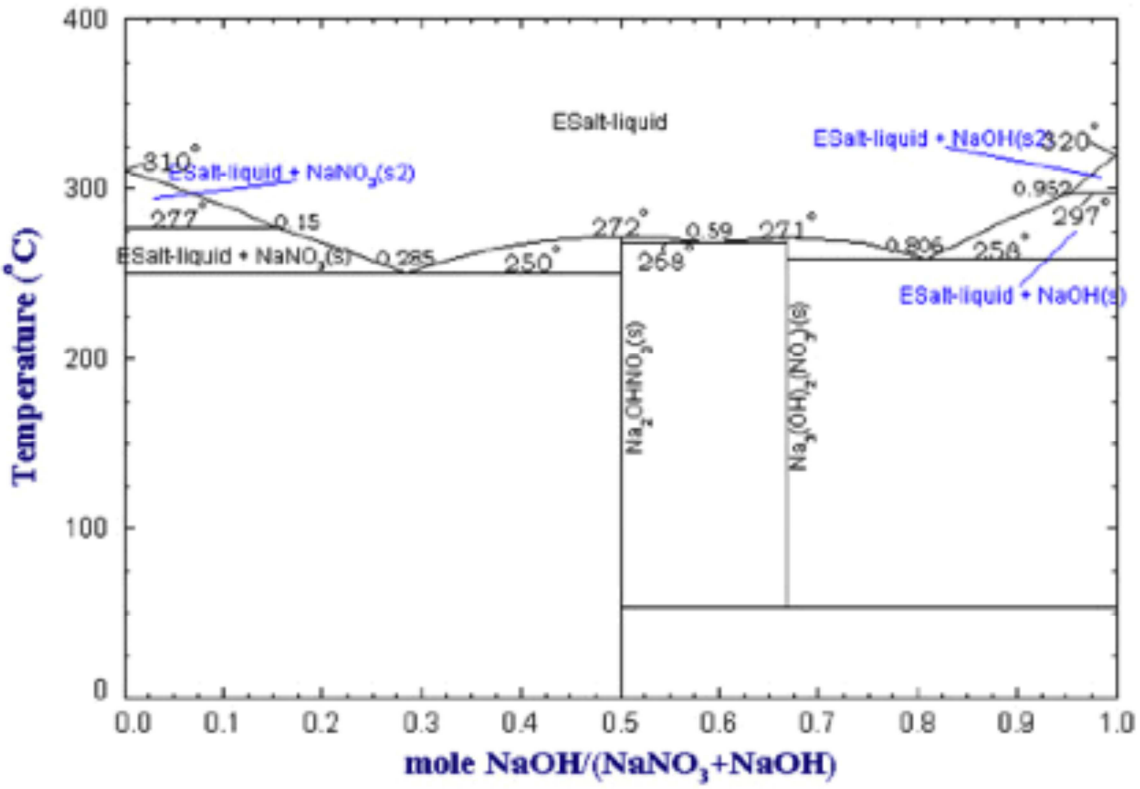

Fig 1 NaOH-NaNO3 binary system phase diagram [1]

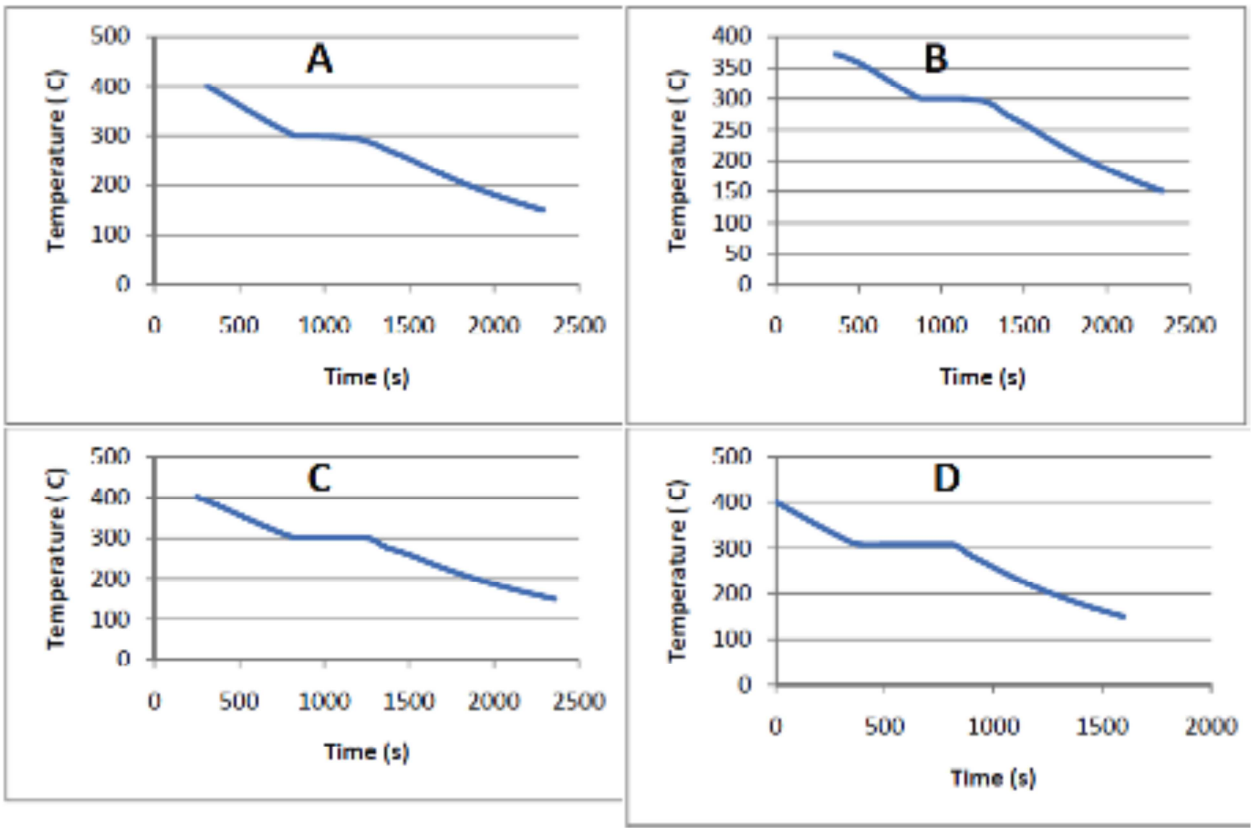

Fig 2 Cooling curves A, B and C: NaNO3(98%), D: NaNO3 (99.999%)
Table 1 Data extracted from fig 2 {A, B and C: NaNO3(98%), D: NaNO3 (99.999%)}

Fig 3A shows the as cast patterns of ingot for general metals and alloys. Grains in the as cast ingots are generally 3 types: equiaxed, columnar and zones in the chill zone which are forming first on the mold's wall. In each metal and alloy depending on the solidification condition and also the composition and type of metal or alloy each zone can be changes or disappears. Our observations on the selected salt system using different ingots such as aluminum, steel, alumina, quartz, and pyrex shows the model in fig. 3B, which means the equiaxed and chill zone are not appearing in the as cast ingot microstructure. However structure of the as cast salt can be dendritic as fig 4 shows, in the as cast sodium nitrate with 98% purity.

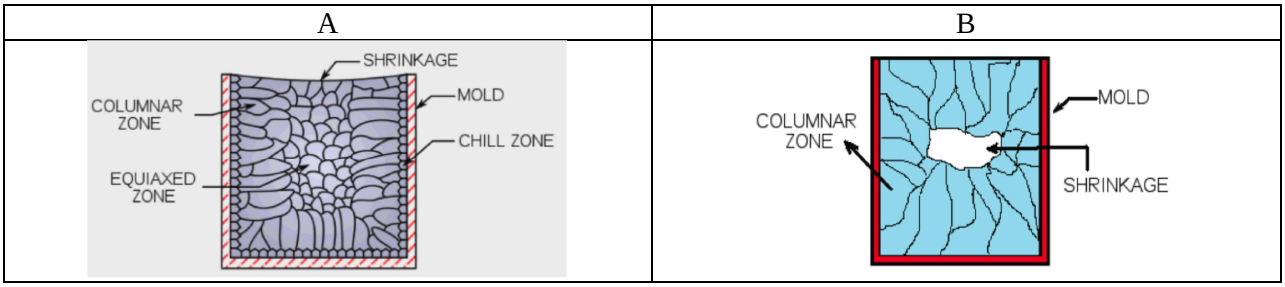

Fig 3 A: General Ingot as cast pattern, B: Salts as cast pattern

Composition	Cooling rate (^{o}C/min)	Transformation Temperature (^{o}C)	Super cooling (C)
NaNO3 (A)	7.6	299.9	0.16
NaNO3 (B)	6.7	299.6	0.103
NaNO3 (C)	7.1	300.6	0.4
NaNO3 (D)	9.4	308	0.84

Fig 4 Ingot as cast pattern for $NaNO_3$ with 98% purity

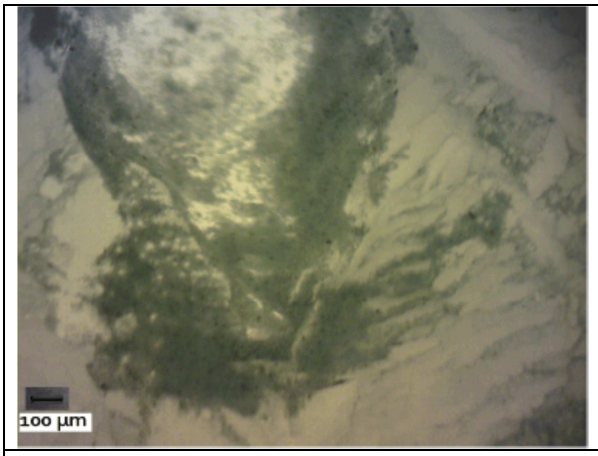

A

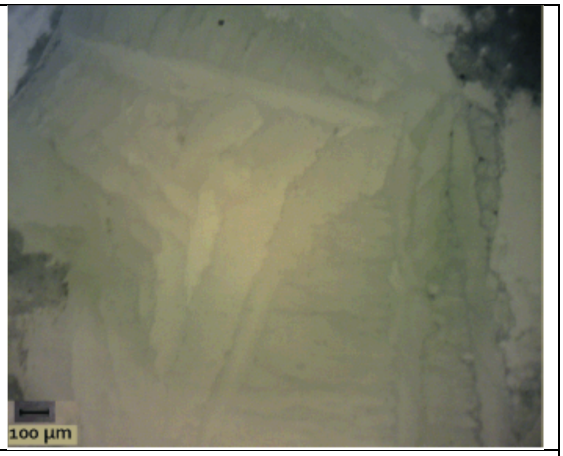

B

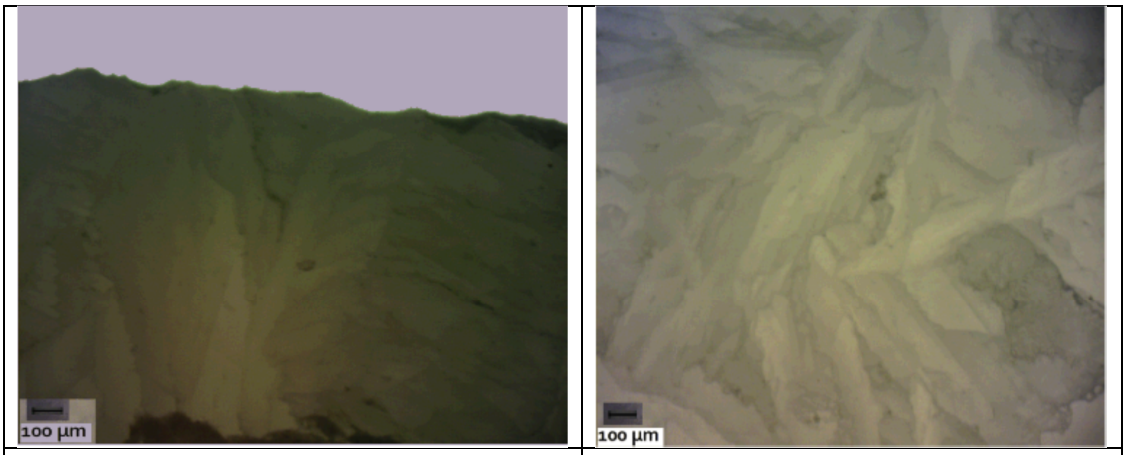

Fig 5 Magnified images of as cast NaNO3 ingot, A: center of the ingot with cavity, B: bottom left of the ingot, C:Top of the ingot, D: Top right of the ingot

Fig 5 shows the magnified cross section of as cast NaNO3 with 98% purity. As it can be seen the columnar zone has occupied the microstructure, with the primary columns elongated from wall to the center and secondary dendritic arms. This dendritic microstructure is because of the presence of 2% impurities. Fig 6 shows the same microstructure but polished from the top of the ingot. In this image different dendritic colonies can be observed with a better contrast.

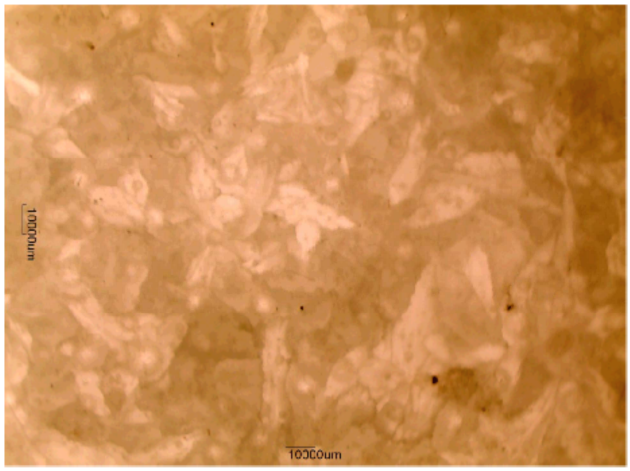

Fig 6 Microstructure of NaNO3 from top of the ingot (Polished structure)

Fig 7 shows the cooling curves for eutectic composition of NaNO3-NaOH with different amount of purity. In fig 7A, B and C cooling curves are related to sodium nitrate and sodium hydroxide with 98% purity and as indicated in table 2, the transformation temperature for these curves is less than the actual eutectic temperature according to fig 1 because of the impurities. In fig 7 D the cooling curve is related to the eutectic composition using sodium nitrate and sodium hydroxide with 99.999% purity, and as table 2 shows the transformation temperature is about 247, which is near to the reported eutectic temperature in fig 1 (250 ^{o}C). Table 2 shows good supercooling temperatures for the C and D compositions. However the amount of supercooling for the A and B compositions is relatively low, and based on the cooling rate it should be higher. The reason can be a non-accurate experiment or problem with thermocouple and those experiments should be repeated.

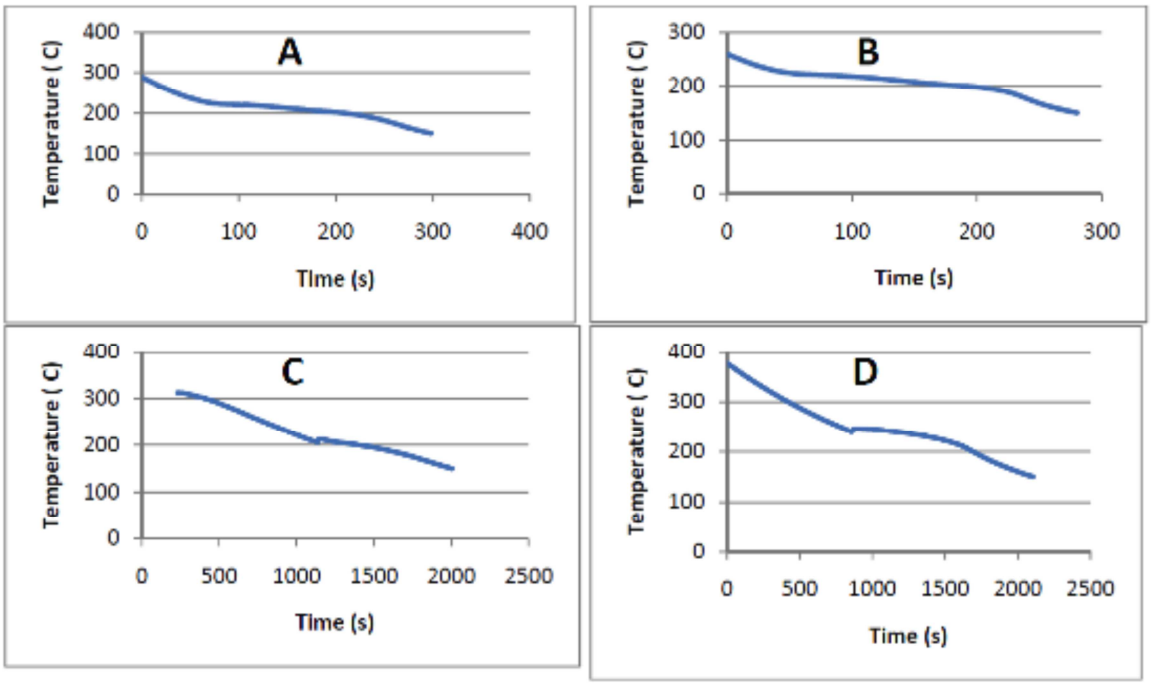

Fig 7 Cooling curves for Eutectic composition of NaNO3-NaOH A, B and C: NaNO3 and NaOH with 98% purity D: NaNO3 and NaOH with 99.999% purity

Composition	Cooling rate (^{o}C/min)	Transformation Temperature (^{o}C)	Super cooling (C)
NaNO3-NaOH (15.6%) (A)	27.8	219.5	1.2
NaNO3-NaOH (15.6%) (B)	23.4	219	0
NaNO3-NaOH (15.6%) (C)	5.5	207	6.8
NaNO3-NaOH (15.6%) (D)	6.5	247	5.9

Table 2 Data extracted from fig 7 {NaNO3-NaOH A, B and C: NaNO3 and NaOH with 98% purity D: NaNO3 and NaOH with 99.999% purity}

Fig 8 shows the cooling curves for hypo eutectic composition of NaNO3- 10wt%NaOH with different amounts of purity. In fig 8A, B and C cooling curves are related to sodium nitrate and sodium hydroxide with 98% purity and the transformation temperatures for these curves are shown in table 3. It is expected for this composition to have two transformation temperatures.
The first transformation happens when the first sodium nitrate solidifies and the second transformation is when the eutectic transformation happens. As it can be seen in the cooling curves, eutectic transformation for all cooling curves A,B and C cooling curves at less than 250 ^{o}C between 230-235 ^{o}C and this temperature off-set is due to the impurities. However the primary solidification of sodium nitrate cannot be detected in these curves. The reason can be the small amount of latent heat of fusion release, which is not sufficient to make a change on temperature or create supercool. In fig 8 D the cooling curve is related

to the hypo eutectic composition using sodium nitrate and sodium hydroxide with 99.999% purity, and as table 3 shows the transformation temperature of 250°C, which is exact reported eutectic temperature in fig 1. Also table 2 shows supercooling temperatures for the A and B compositions more than C and D and the reason is because of the higher cooling rate.

Fig 9 A, B and C: Dendritic structure of $NaNO_3$-10wt%NaOH, D: microstructure change from sharp dendrites to fine rounded dendrites when $NaNO_3$ and NaOH used in the NaNO3-10%NaOH composition are pure (99.999%)

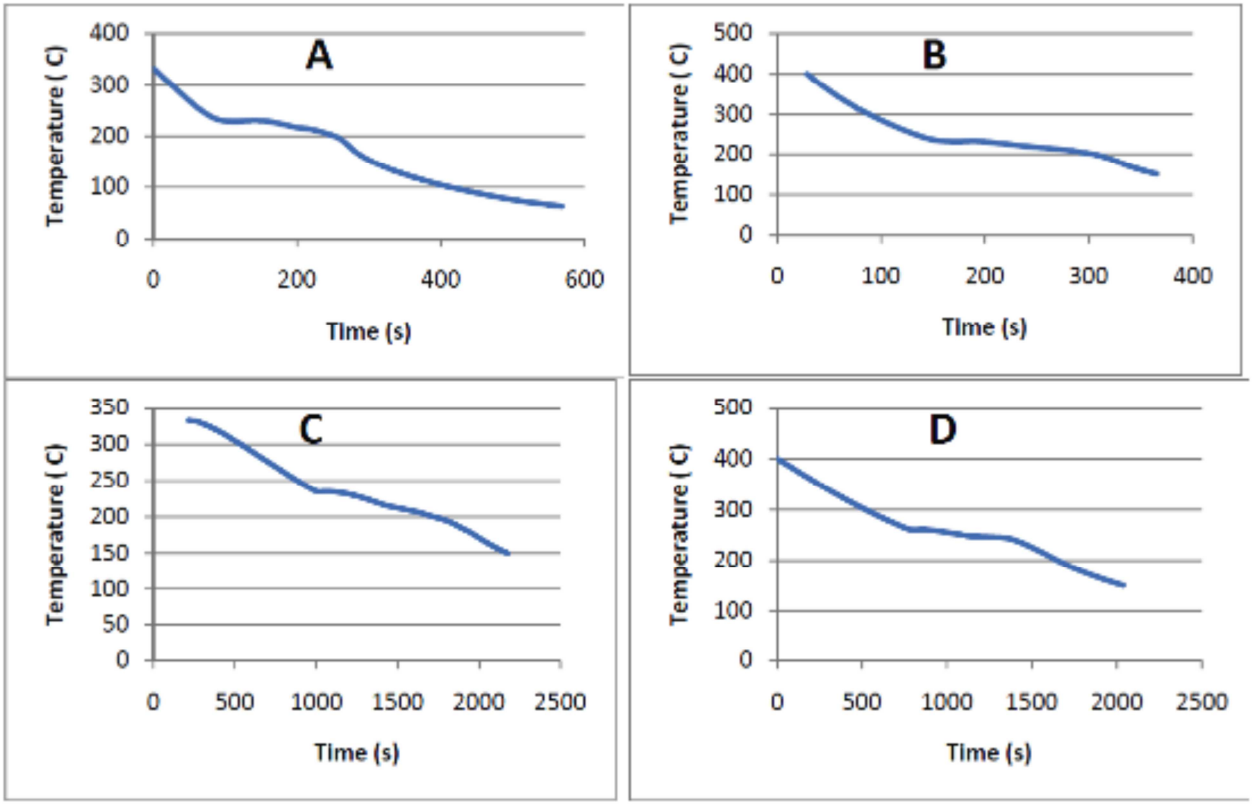

Fig 8 Cooling curves for NaNO3-10wt%NaOH composition of NaNO3-NaOH A, B and C: NaNO3 and NaOH with 98% purity D: NaNO3 and NaOH with 99.999% purity

Composition	Cooling rate (°C/min)	Transformation Temperature (°C)	Super cooling (C)
NaNO3-NaOH (10%) (A)	35.9	230	1.6
NaNO3-NaOH (10%) (B)	44.5	233	1.5
NaNO3-NaOH (10%) (C)	5.6	235	0.6
NaNO3-NaOH (10%) (D)	7.4	250	0.3

Table 3 Data extracted from fig 8 { NaNO3-NaOH A, B and C: NaNO3 and NaOH with 98% purity D: NaNO3 and NaOH with 99.999% purity}

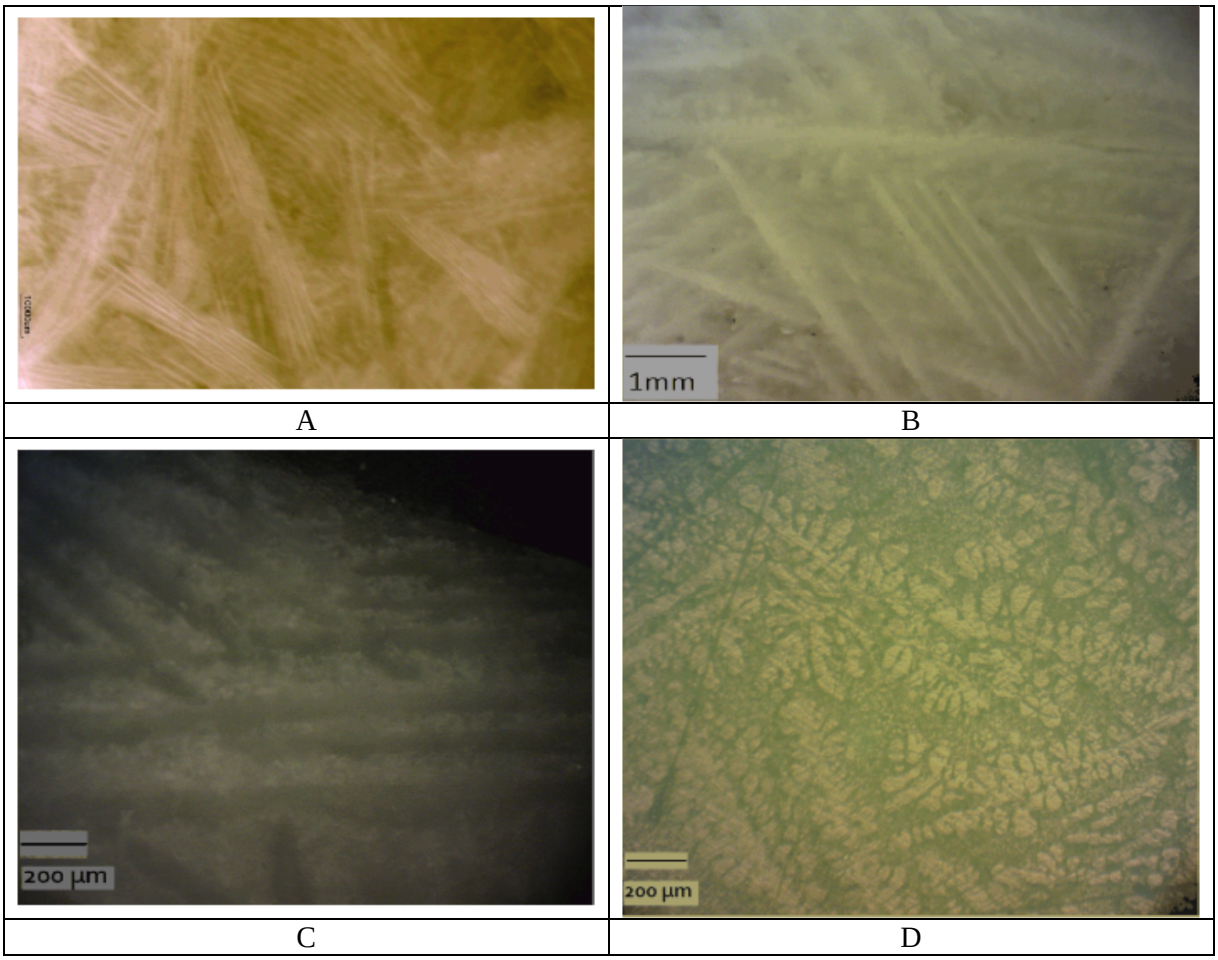

Fig 9 A, B and C: Dendritic structure of $NaNO_3$-10wt%NaOH, D: microstructure change from sharp dendrites to fine rounded dendrites when $NaNO_3$ and NaOH used in the NaNO3-10%NaOH composition are pure (99.999%)

It was pointed out in background studies that if the liquid is at a lower temperature than the interface, dendritic growth is observed. This implies that an initially smooth interface is unstable in the presence of a temperature inversion. In a smooth interface under ordinary growth conditions and supercooled interface a ribbon shaped crystal with its two flat surfaces parallel to a closely packed plane of structure may forms [34]. Fig 9 shows the different structures based on the cooling curves in fig 8. As it can be seen the morphology of the primary dendrites formed in the microstructure of the hypo eutectic composition changes with the amount of impurities in the microstructure. Figure 9 A, B and C show the same needle type dendrites but different sizes, and as purity of the composition increases the morphology of the dendrites totally changes to a more round type dendritic structure in fig 9-D. The supercool temperatures and cooling rates does not have any effect on the shape of primary dendrites but changes the size of the dendrites. As it can be seen in figure 9 the higher the rate, results to a finer dendritic structure. The type of dendrite structure in fig 9 A, B and C can be what reported in aluminum alloys [2-3], called as feather crystals and feather growth. The crystals shown in this figure appear to resemble ribbon crystals in that they always contain twin planes, but it is not obvious why a twin mechanism should come into play in a material in which the interface is believed to be diffuse. It is possible that the feather crystals grow only when the supercooling at the interface is so small that the diffuseness of the interface is insufficient to allow new layers to form. This explanation is not supported by the observation that feather crystals do not occur unless the conditions are such that growth is fast. Although the significance of this research is based on the primary formed dendrites and their morphology, since in solar power plant heat exchanger the solidification only happens partially and never reaches to the eutectic point, recognition of

the eutectic structure is important in order to understand the difference between the primary dendrites and dendrites lie in the eutectic structure. As discussed before the smooth interface is caused because of the completion of the atomic layers, and in this type of structure eutectic structure is irregular and hard to detect. Also because of the supercooling formation of divorced eutectic happens as it is indicated in fig 10.

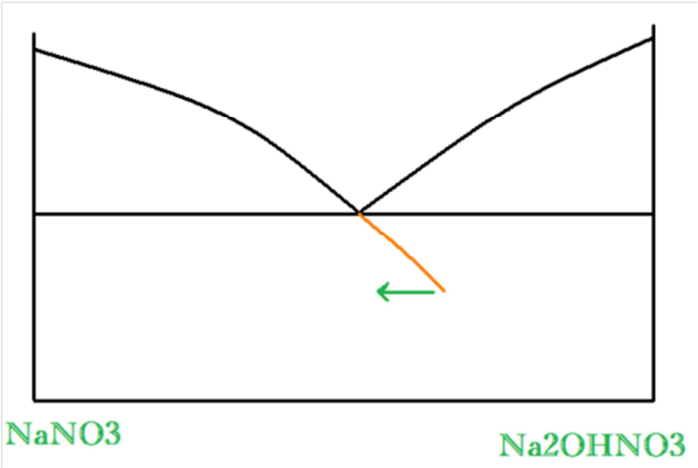

Fig 10. NaNO3-NaOH Phase Diagram

Fig 11 shows a microstructure of a divorce eutectic in the composition of NaNO3-10%NaOH with purity of 99.999%. The dark parts are sodium hydroxide and it can be seen they have absorbed some moisture due to the nature of being so hygroscopic.

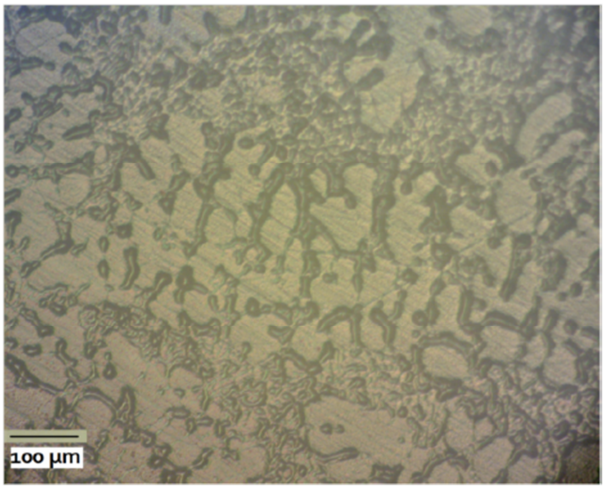

Fig 11 Divorced Eutectic structure in the composition of NaNO3-10wt%NaOH with purity of 99.999%

Appendix 1 discusses viscosity of salt mixture at near freezing temperature. There is very scant data on viscosity of salt near melting and freezing, because it is difficult to measure. Fig 12 and 13 show our initial attempt to measure viscosity of a eutectic and a hypo eutectic composition of NaNO3-10wt%NaOH. In fig 12 viscosity has been measured in the temperature range right above the freezing point. The freezing point for the first solidified eutectic is 260C according to phase diagram in fig 1 but because of the supercooling and also temperature reading off-set in this chart no solidification has occurred. The tread line shows the linear viscosity change with temperature change. As it can be seen viscosity of the molten salt changes between 1-2 cp. By increasing the temperature the viscosity decreases as in fig 13 and gets more near to 1 cp. The behavior of molten salt's viscosity is what expected according to [4](see Appendix 1) .

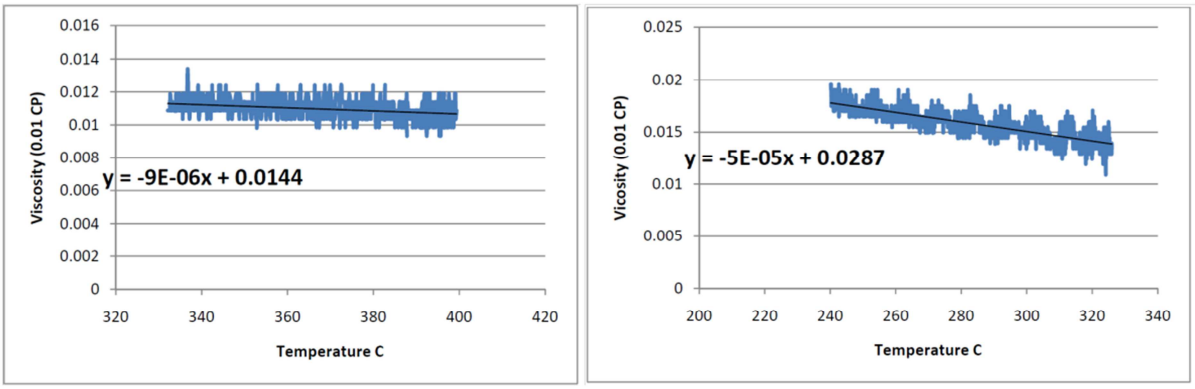

Fig 12 and 13 Viscosity-Temperature chart of the eutectic and hypo eutectic composition of NaNO3-10wt%NaOH in the temperature range of right above the freezing point

Measuring viscosity at or near freezing or melting temperature is challenging. Figure 14 shows the viscosity of sodium nitrate salt near melting temperatures (300 to 308 C). These measurements were at conducted at NREL by Dr. Anne Starace.

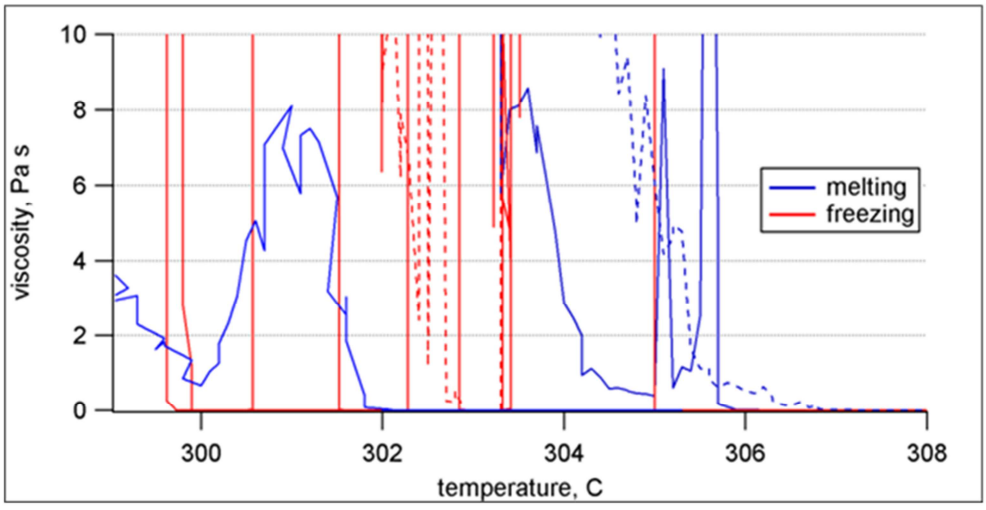

Figure 14. Measurement of viscosity near freezing and melting temperatures for NaNO3

Section 6
Design of Laboratory Scale Prototype

Focus of this Section

This section focuses on the design of the experiment apparatus for studying the heat transfer performance in latent heat storage systems. The report begins with a baseline analysis balancing predicted overall heat transfer coefficient and solidification with heat exchanger area. After this, more detailed analysis is presented to analyze the effects of tube size on Reynolds number, pressure drop, % solidification, etc. The purpose of this is to establish a baseline of calculations for further detailed design to follow. The analysis assumes cross flow, which should be analogous to a baffled shell and tube heat exchanger.

Introductory Analysis

To begin our analysis we will present a baseline energy balance calculation. We balance the overall heat transfer rate with the energy it takes to bring the salt down to melting temperature and achieve a solid fraction of 20%. For the purposes of this calculation we assume tubes of 0.375" OD, and a channel cross section of 10 diameters square (i.e., 3.75" x 3.75"). We account for 50% of this area being blocked by tubes giving us a cross sectional area, A_c, of .009 m^2*50%. We also assume an overall ΔT of 15 degrees Celsius between salt and tube walls, and an inlet superheat of 5 degrees Celsius.

$$\dot{Q} = hA_s\Delta T = \dot{m}\left(C_p T_{superheat} + H_f \varphi\right) = \left(\rho A_c V\right)\left(C_p T_{superheat} + H_f \varphi\right)$$

h (W/m^2K)	500
ΔT (C)	15
C_p (kJ/kgK)	1.821
$T_{superheat}$ (C)	5
H_f (kJ/kg)	174
ϕ (% Solid)	20%
ρ (kg/m^3)	2260
A_c (m^2)	.009*50%

From this we are left two independent variables: heat exchanger surface area A_s and salt velocity V. If we assume a velocity of 1 m/s (Re_D=8300), Q works out to 450 kW, which leads us to a heat exchanger area of 60 m^2. This means for an array of 40 cooled tubes we would need over 525 passes to achieve the desired solid fraction. Alternatively, we could achieve the desired 20% solid fraction at only 14 kW if we decreased the salt velocity to 0.03 m/s; however in this case the salt-side Reynolds number would be only 250.

Importance of Reynolds Number

The capability of operating at high Reynolds number is an important functionality for this apparatus for two major reasons:

(i) To ensure that we can produce the hydrodynamic forces that will be necessary to achieve "flaking" of the salt off of the tube. The larger the range of Reynolds numbers we can test, the larger the range of coatings we will be able to test. Even if our coatings fail to flake at industrially viable Reynolds numbers, if we can prove that flaking will occur at higher Reynolds numbers this will be proof that our concept is viable. From a scientific perspective if we could hit a high enough Reynolds number to flake off of a plain or coated steel tube, we could begin to perform a thorough study in which we could possibly come up a with a formula to relate coating surface energy to Reynolds number necessary for flaking. This would make heat exchanger design for the full scale system very simple. On the other end, if we don't give ourselves the capability of high Reynolds numbers we may fail to create the flaking phenomenon at all.

(ii) Scaling to match full-size heat exchangers: Based on initial familiarity with typical full-scale heat exchangers involving molten salt, we expect that a typical Reynolds number is in the range of 20,000. Also, typical convection design curves for staggered tube banks and shell & tube heat exchangers show a transition in behavior at around $Re_D \approx 1{,}000$, in terms of both pressure drop and heat transfer [ref. *Perry's ChemE Handbook*; Zukauskas in Hartnett & Irvine *Adv. Heat Transf*]. Therefore, to be able to match the approximate operating conditions of a full-scale heat exchanger, it is important for this apparatus to be capable of operating in the ReD range of several 1,000 at the very least, and with a strong preference to reach the range of 20,000+.

Heat Exchanger Design

The main goal of the system is to determine the salt side convection coefficient. Figure 1 shows a schematic of the thermal resistance network of the heat exchanger during solidification. The salt side convection coefficient contains two terms, the external convection as well as conduction through any solid salt on the surface. As shown in equation 2, we assume the contribution of the solid salt conduction is negligible, as well as conduction through the thin stainless steel tube. Effects of any solid salt layers forming will be captured in the h_{salt} measured and the stainless steel tube is too thin to play a significant role in the measurement. That leaves only $h_{coolant}$ and h_{salt} as contributors to the overall heat transfer coefficient. Assuming we can make $h_{coolant} >> h_{salt}$, a measurement of the overall heat transfer coefficient will give us a measure of how effectively the salt can transfer heat under real heat exchanger conditions. By measuring the flow rates and inlet and outlet temperatures of each system, we can determine the Log Mean Temperature Difference and calculate the overall heat transfer coefficient.

To determine how to scale the system down, we must first look at the configuration of the full scale system. In the full scale system hot salt will come from the superheat heat exchanger slightly above the melting point of the salt. This salt will be pumped through a shell and tube heat exchanger where the heat from the salt will boil steam on the inside of the tubes. This steam will be diverted to a turbine, which will then produce electrical power. System calculations performed by Anoop Mathur show that a potential heat exchanger design would utilize 1" diameter tubes, with a salt velocity of approximately 3 feet per second. We scaled these conditions to dimensionless Reynolds and Nusselt numbers to help determine the sizing requirements for our scaled system.

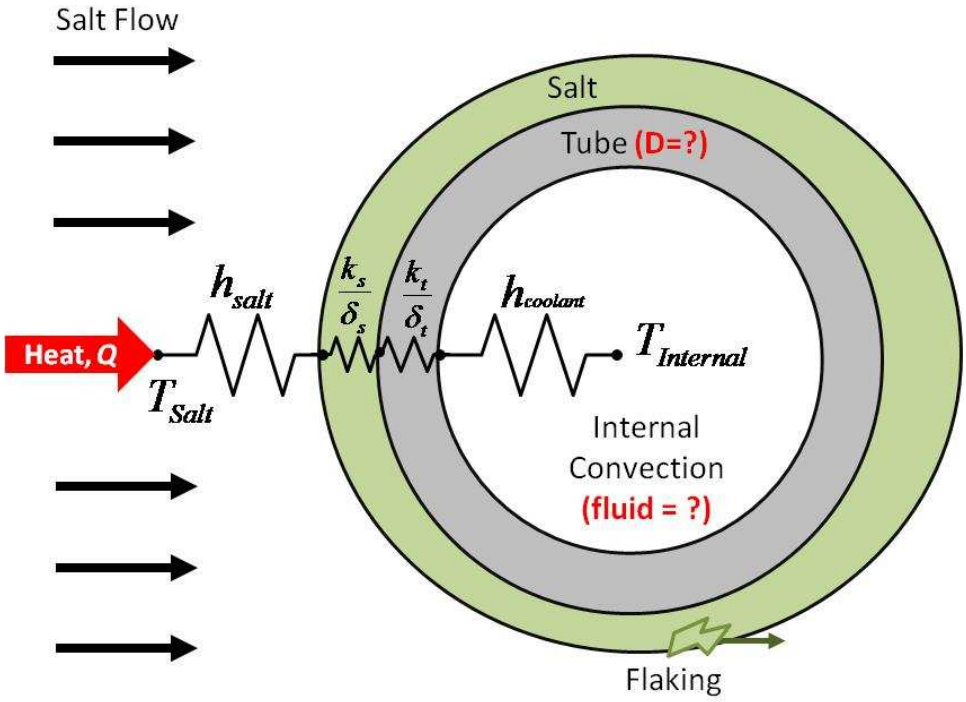

Figure 1: Schematic of Heat Transfer during Solidification on Heat Exchanger Tube

$$\frac{1}{U} = \frac{1}{h_{Salt}} + \frac{\delta_s}{k_s} + \frac{\delta_t}{k_t} + \frac{1}{h_{coolant}} \qquad (2)$$

Best Case, $\delta_s \to 0$ — Thin SS Tube

In the scaled system, it is highly beneficial to avoid steam generation as the pressure of saturated steam at the melting point of the salt is approximately 1250 psi. This creates a highly hazardous situation as the system would have be extremely meticulously designed in order to avoid a high pressure leak of steam that could create extreme hazards when combined with the molten salt. Therefore it is highly preferential to find another heat transfer fluid that will provide effective heat transfer under safer conditions.

Heat Transfer Fluid Selection

Five different heat transfer fluids were analyzed under sample conditions to analyze their effectiveness as a heat transfer medium. A ¼" tube with an L/D ratio of 30 was utilized for this analysis. Compressed air and helium were analyzed at a pressure of 60 psi. Figure 2 shows the pressure drop versus convection coefficient for each fluid and Figure 3 shows the flow rate versus convection coefficient for each fluid. From these graphs it was determined that Therminol© and compressed helium were the most effective solutions.

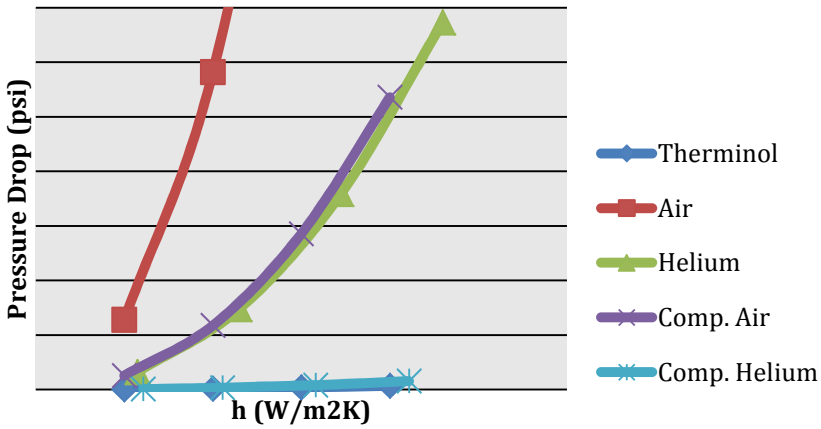

Figure 2: Sample System Pressure Drop vs. Convection Coefficient for Different Heat Transfer Fluids

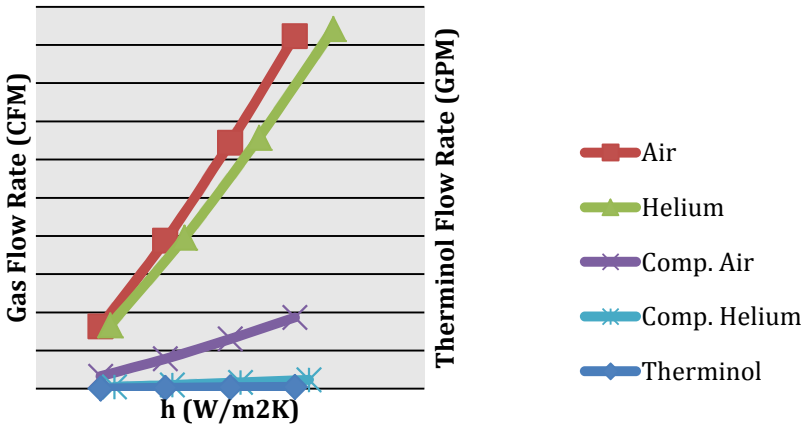

Figure 3: Sample System Flow Rate vs. Convection Coefficient for Different Heat Transfer Fluids

From here, a basic design for each system was laid out and the pros and cons of each system analyzed. Compressed helium is good because it is easy to work with, simple to implement (no special research required), leaks are easy to deal with and tolerate, and the overall system complexity is reduced. However, it is not normally used in industry, is more expensive, and is still a pressurized system. Therminol is beneficial due to fact that the system does not have to be pressurized, higher heat transfer rates are more easily achievable, it is less expensive, and it is widely accepted in industry. The Therminol system is much more complicated though, more safety issues are involved in the design, leaks are more difficult to tolerate, and a good amount of research is necessary to ensure proper implementation. In the end Therminol was chosen because of its acceptance in industry, and how much cheaper the system is.

Figure 4 shows the pump work required versus heat transfer coefficient for each fluid. The helium compressor requires significantly more power and therefore the ratio of helium compressor to Therminol pump cost is approximately 8:1 ($10,000 vs. $80,000).

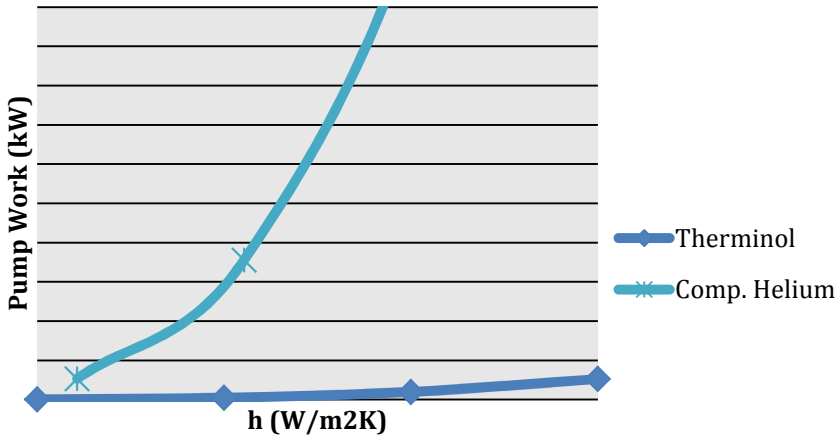

Figure 4: Pump Work vs. Convection Coefficient for Therminol and Compressed Helium

Heat Exchanger Design

Once a heat transfer fluid was selected, it was necessary to perform detailed scaling calculations to maximize the effectiveness of the system while utilizing as small a scale as possible. In order for the system to perform effectively there are a number of factors that must be carefully balanced. The first is high oil heat transfer. The higher this is, the easier it will be to isolate the actual salt heat transfer coefficient. Next is a low pressure drop, which allows us to utilize smaller pumps. A high Reynolds number on the salt side is beneficial as it will produce larger hydrodynamic forces that may help flake salt off of the tube. Another very important factor is the change in solid fraction that can be achieved through the heat exchanger. The higher the change in solid fraction that we can achieve, the better the industrial readiness of the system being tested.

A staggered tube bank was chosen as the best physical design due to the fact that the geometry is well understood, and heat transfer modeling becomes very simple. This geometry is very true to industry practice and also maintains the external cross-flow orientation that an industrial shell and tube heat exchanger would have. All calculations assume a 4x10 staggered tube bank. Equations 2-4 show some of the general equations used in these calculations. Any other equations used can be found in Incropera and Dewitt's Introduction to Heat Transfer [6].

$$Re_{D,max} = \frac{\rho V_{max} D}{\mu} \quad (3)$$

Where $Re_{D,max}$ is the maximum Reynolds number through the tube bank, ρ is the density of the fluid, V_{max} is the maximum velocity through the tube bank, D is the diameter of the tubes, and μ is the dynamic viscosity of the fluid.

$$\overline{Nu}_d = 1.13 C_1 Re_{d,max}^{m} Pr^{\frac{1}{3}} \quad (4)$$

$$\begin{bmatrix} N_l \geq 10 \\ 2000 \leq Re_{D,max} \leq 40{,}000 \\ Pr \geq .7 \end{bmatrix}$$

$$\Delta p = N_L \chi \left(\frac{\rho V_{max}^2}{2}\right) f \quad (5)$$

The length of tube to tube diameter ratio was held to a constant value of 10. Pitch between the tubes in both the longitudinal and transverse direction was twice the diameter. All values shown are on a per pass basis, once calculations were finalized, passes were added where necessary to generate the desired results.

A series of figures is presented, followed by a table summarizing the calculations. The salt side of the loop was analyzed first. Figure 5 shows the pressure drop through the heat exchanger on the salt side. As the tube size decreases, the pressure drop increases significantly. Figure 6 shows the maximum Reynolds number achievable at 140 GPM (this was used as a design point because it is the maximum achievable flow rate achievable by an older pump that we had.) Figure 7 shows the salt solid fraction achievable per pass versus flow rate in GPM. Figure 8 shows the cooling rate required to balance the solidification and cooling versus tube diameter. This was an extremely important design point as it plays a large role in determining the steady-state load on the heating system.

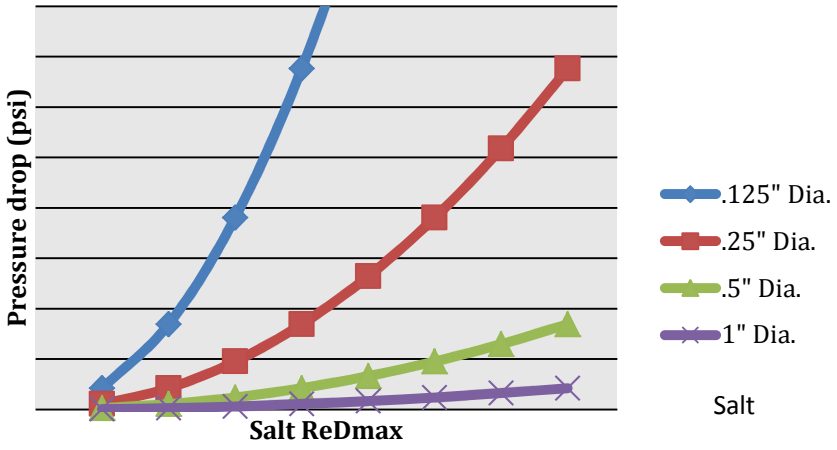

Figure 5: Salt Pressure Drop vs. ReDmax for Different Tube Sizes

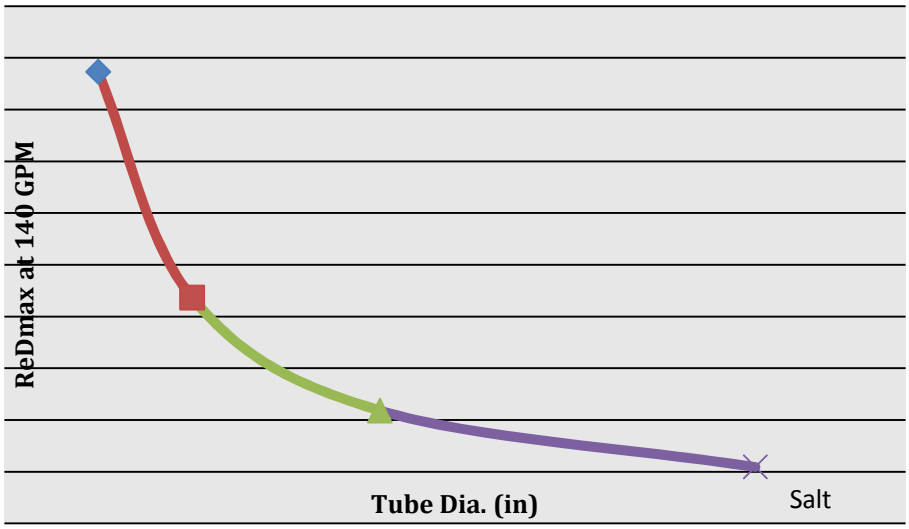

Figure 6: Salt ReDmax at 140 GPM Flow Rate vs. Tube Diameter

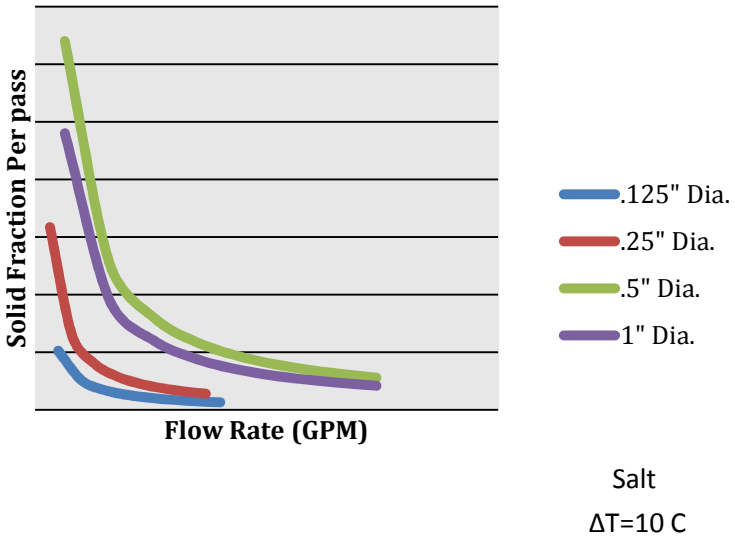

Figure 7: Salt Solid Fraction per Pass vs. Flow Rate

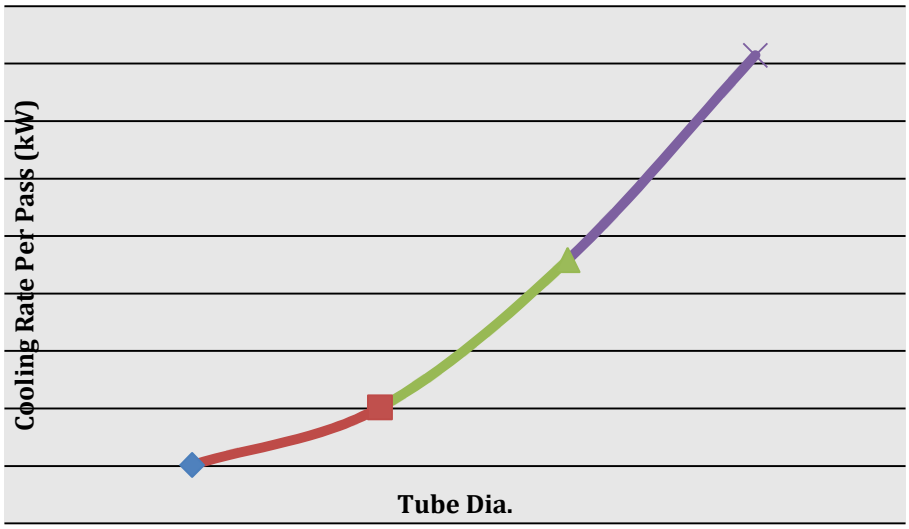

Figure 8: Cooling Rate Required Per Pass vs. Tube Dia.

The Therminol Side shows similar trends. Figure 9 shows the Therminol pressure drop per pass versus Reynolds number for various tube sizes. The pressure drop increases with decreasing tube size at equivalent Reynolds Numbers. Figure 10 shows flow rate vs. Reynolds number for various tube sizes. Lower Reynolds numbers are associated with the same flow rate as tube diameter increases. Figure 11 shows the oil temperature rise versus Reynolds number for various tube sizes. The differences here are minor, but smaller tube sizes will develop larger temperature gradients and will be more easily measured. Figure 12 shows the heat transfer ratio vs. Reynolds number for various tube sizes. As tube size decreases the heat transfer ratio increases, allowing for a cleaner salt side heat transfer calculation. Figure 13 shows heat transfer ratio vs. flow rate for various tube diameters at maximum power condition from the pump curves for three different prospective pumps. It becomes even more apparent in this figure that it is much easier to achieve high heat transfer ratios with smaller tube diameters than with larger ones. Figure 14 shows the maximum achievable Reynolds number when utilizing the smallest chosen pump vs. tube diameter.

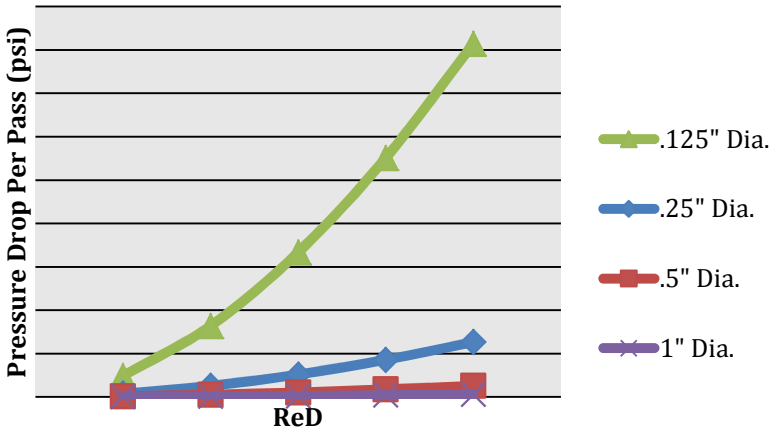

Figure 9: Therminol Pressure Drop per Pass vs. ReD for Different Tube Sizes

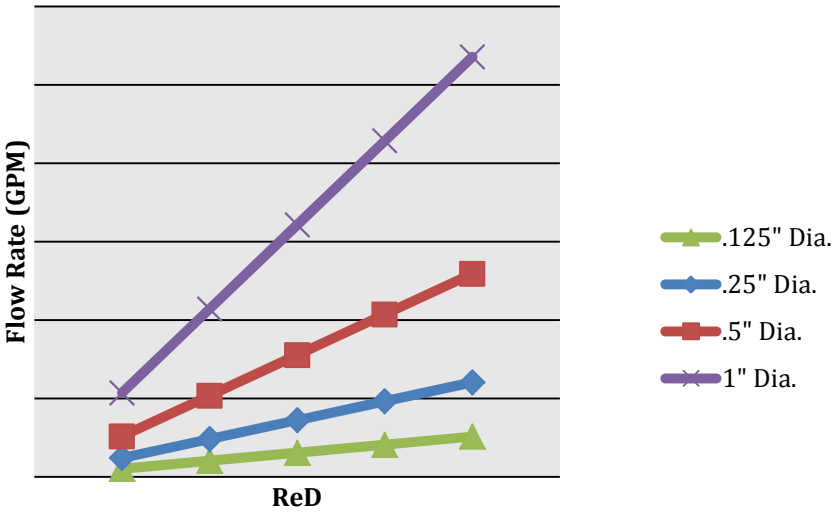

Figure 10: Therminol Flow Rate vs. ReD for Different Tube Diameters

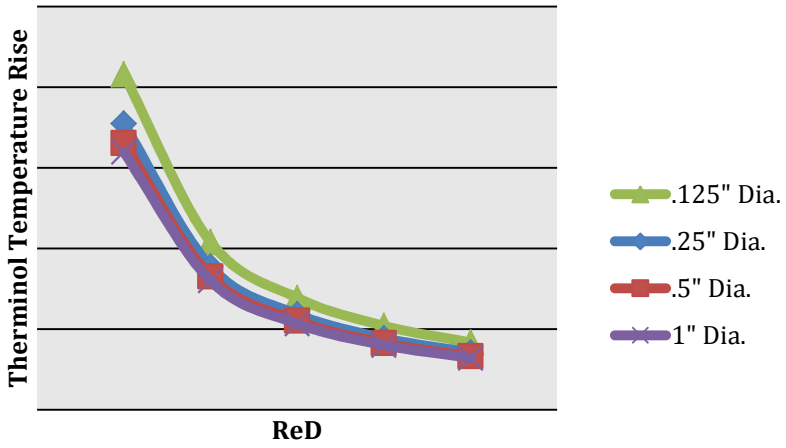

Figure 11: Therminol Temperature Rise vs. ReD for Different Tube Diameters

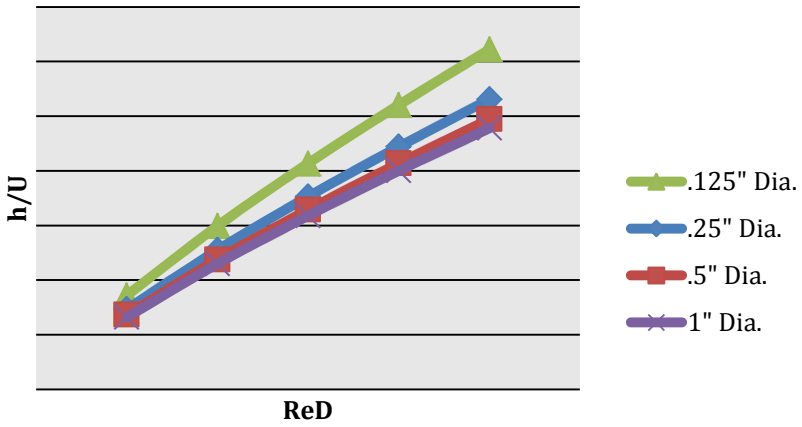

Figure 12: Heat Transfer Ratio vs. ReD for Different Tube Diameters

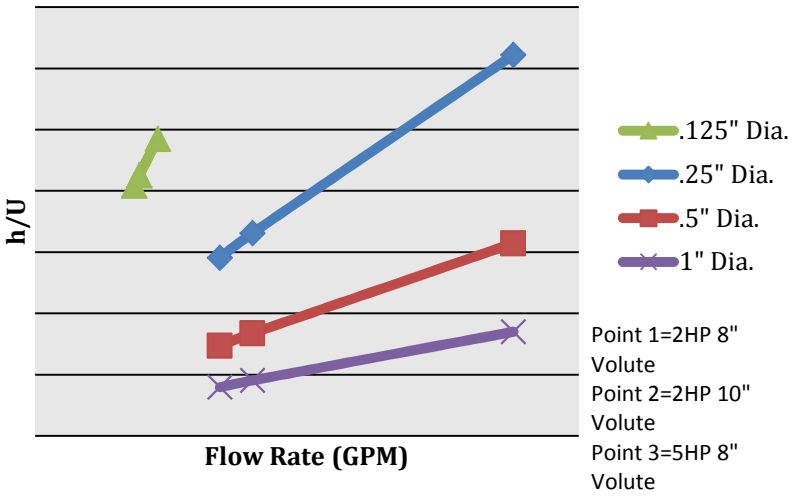

Figure 13: Heat Transfer Ratio vs. Flow Rate for Different Pumps and Different Tube Sizes

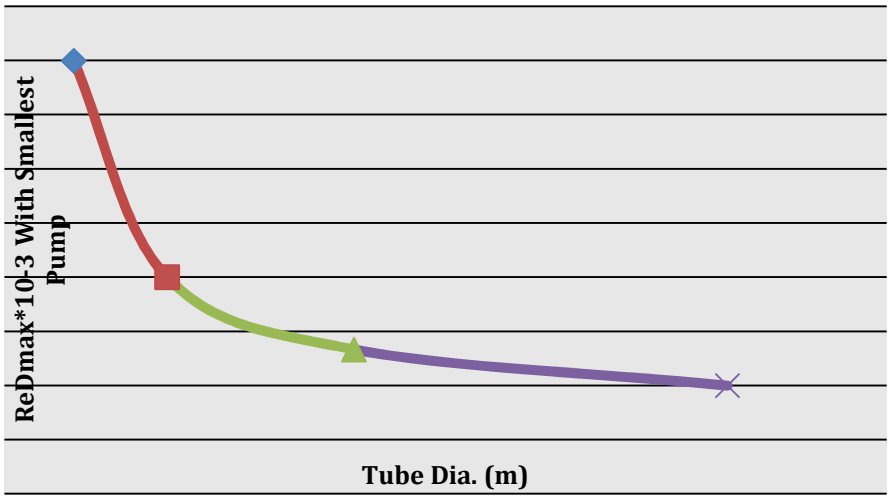

Figure 14: Therminol ReDmax Achievable With Smallest Pump vs. Tube Diameter

Table 1 shows a summary of these calculations for specific design points. The salt calculations show how the properties vary under a constant 140 GPM flow rate through the heat exchanger. For the Therminol calculations the heat transfer ratio was held to a constant of 10, and the other values were analyzed accordingly. Finally, the cooling rate and an overview of the pump calculations are tabulated.

Table 1: Tube Diameter down Selection Table

	Tube Diameter	1/8”	¼”	3/8”	1/2"	1"
Salt (140 GPM)	Pressure Drop Per Pass (psi)	740	18	8	5	2
	ReDmax at 140 GPM	43000	22000	16000	11000	5500
	ΔSolid Fraction Per Pass at 140GPM	0.02	0.04	.06	0.08	0.17
Therminol h/u=10	Pressure Drop Per Pass (psi)	1.2	0.25	.12	0.05	0.01
	GPM	8	20	30	40	80
	ΔT per pass	52	35	34	33	32
Overall	Q (kW)/Pass ΔT=10 (C)	50	100	150	200	400
8" Volute 2HP	h/u Max	40	28	22	15	7
10" Volute 2HP		43	33	25	17	9
8" Volute 5HP		49	62	47	31	17

From this information, it was decided that 3/8” was the optimum diameter to be utilized for this system. Figure 15 shows a CAD rendering of the final design. In order to get high signal to noise ratio as well as allowing for higher solid fractions, a six pass design on the salt side was chosen. A single pass design on the oil side was chosen to simplify design and protect the oil from overheating.

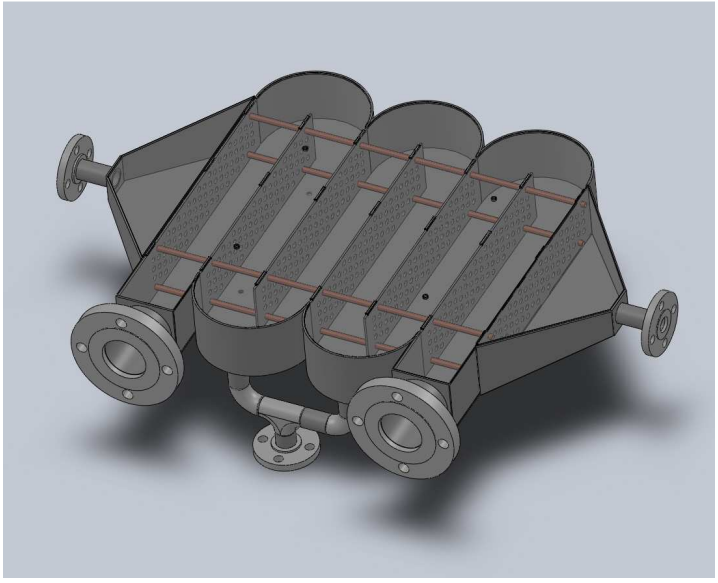

Figure 15: Rendering of Heat Exchanger CAD Design

Once the heat exchanger was designed, the rest of the system was developed to supply it. A 20 horsepower molten salt pump was purchased from Friatec©, a 2 horsepower magnetic drive hot oil pump was purchased from Dickow pumps, and Reflexx Designs was commissioned to oversee the construction of the apparatus. Figure 16 shows a rendering of the CAD model that was developed. Detailed heat loss calculations were performed in order to properly size the heating and cooling systems for the apparatus.. Once the losses were determined, a much larger heating capacity was installed on the system to allow for more dynamic operation. The final system utilizes 22 kW of heaters for the salt tank and 12 kW of heaters for the oil recirculation system. Figure 17 shows a picture of the final assembled system before final wiring and insulation. Much care had to be put in to ensure proper insulation and heating of the salt recirculation system. If the entire system is not maintained above the melting point of the salt the salt can solidify and cause blockages in the pipes. This was a major practical hurdle in the construction of the system and led to many of the delays in system operation. To monitor system readiness for operation as well as to perform the heat transfer measurements, an extensive instrument and control system was developed. Figure 18 shows a schematic of the instrumentation that was installed on the system. Figures 19 and 20 show schematics of the oil and salt systems individually. A pair of RTD's was utilized at each inlet and outlet of both recirculation systems to achieve higher accuracy at these critical measurement points. Where measurements were not as critical thermocouples were utilized due to their lower cost. A total of 19 thermocouples, 8 RTD's, and 2 flow meters were installed on the system to monitor system operation and perform heat transfer measurements. A vortex shedding flow meter from Sierra Instruments was utilized on the salt system due to its high temperature resistance and relative insensitivity to fluid properties. On the oil system a high temperature piston-style flow meter was utilized on the oil side from Lake Flow Meters.

Once the apparatus was finished, the individual system components were tested and optimized to ensure optimum performance during testing. This was an extremely intensive process due to the unpredictable nature of the system as the system undergoes thermal cycling. Many of the initial heaters failed due to warping of the salt tank, and new immersion heaters had to be retrofitted on the system to enhance the heating capacity of the system. Similarly, the Therminol system required much more heat than anticipated and therefore required an additional circulation heater to be retrofitted on the system. Furthermore, the vapor pressure of Therminol is positive at high temperature and created more fumes than anticipated. Therefore a recovery/venting system was implemented to reduce the fumes created and vent any fumes that were generated away from workers.

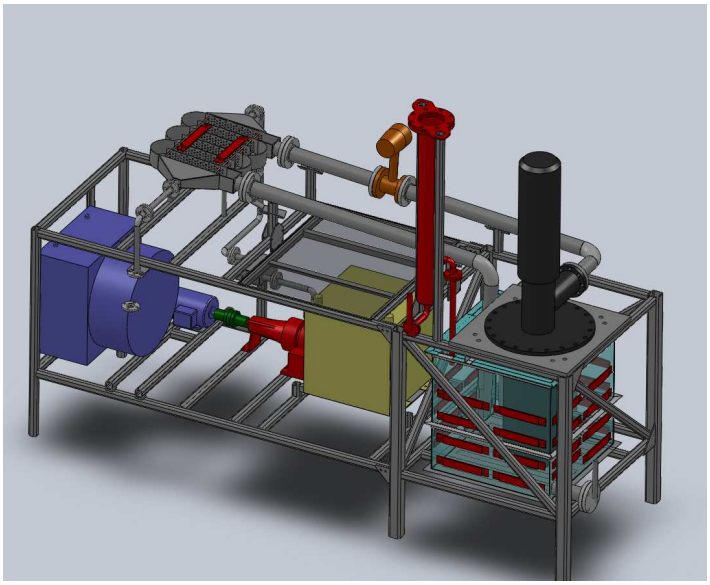

Figure 16: Rendering of Entire System CAD Design

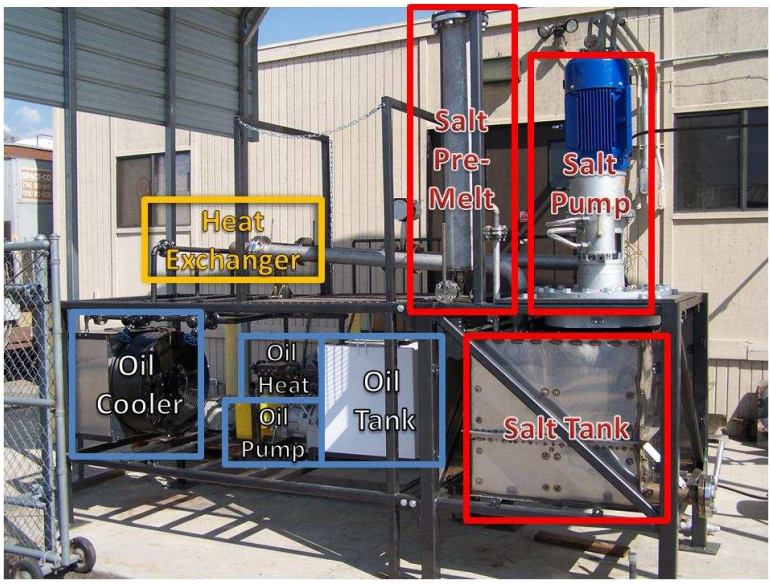

Figure 17: Image of Built System with Components Labeled

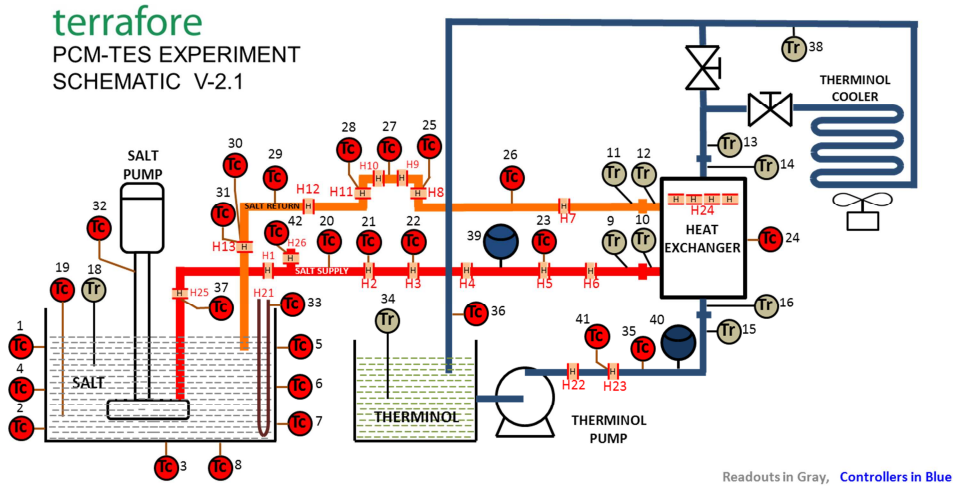

	Tc1	Upper Strip Heater TC		Tr12	HX Salt Return Near Side RTD	19	Tc24	HX Wall TC (H24)	4	Tc35	Therminol Hot TC (H22)
	Tc2	Lower Strip Heater TC		Tr13	HX Therminol Supply Far Side RTD	13	Tc25	Zone-4 TC (H7)		Tc36	Therminol Return TC
	Tc3	Bottom Strip Heater TC		Tr14	HX Therminol Supply Near Side RTD	12	Tc26	Zone-4 TC (H7-H8)	3	Tc37	Zone-1 TC (H25)
	Tc4	Salt Tank Wall TC		Tr15	HX Therminol Return Far Side RTD	14	Tc27	Zone-5 TC (H9,H10,H11)		Tr38	Therminol Cooler Return
	Tc5	Salt Tank Wall TC		Tr16	HX Therminol Return Near Side RTD	15	Tc28	Zone-5 TC (H11)		39	Salt Flow Meter
	Tc6	Salt Tank Wall TC		Tr18	Salt Tank Shallow RTD	16	Tc29	Zone-6 TC (H12-H13)		40	Therminol Flow Meter
	Tc7	Salt Tank Wall TC		Tc19	Salt Tank Deep TC	17	Tc30	Zone-6 TC (H13)	6	Tc41	Therminol Band Heaters (H23)
	Tc8	Salt Tank Bottom TC	8	Tc20	Zone-1 TC (H1-H2)		Tc31	Zone-6 TC (H13)	5	Tc42	Burst Disc Housing (H26)
	Tr9	HX Salt Supply Far Side RTD	9	Tc21	Zone-1 TC (H2)		Tc32	Salt Pump Housing TC			
	Tr10	HX Salt Supply Near Side RTD	10	Tc22	Zone-2 TC (H3)	1	Tc33	Salt Heater TC (H21)			
	Tr11	HX salt Return Far Side RTD	11	Tc23	Zone-3 TC (H5)		Tr34	Therminol Tank RTD			

Figure 18: Instrumentation Schematic for Flow Loop

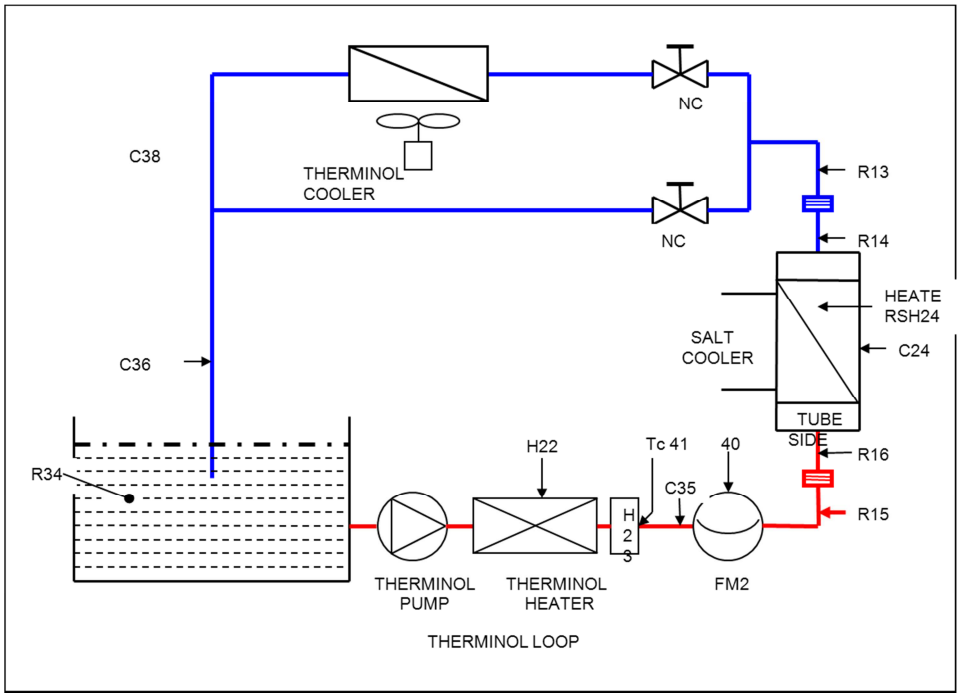

Figure 19: Therminol Loop Schematic

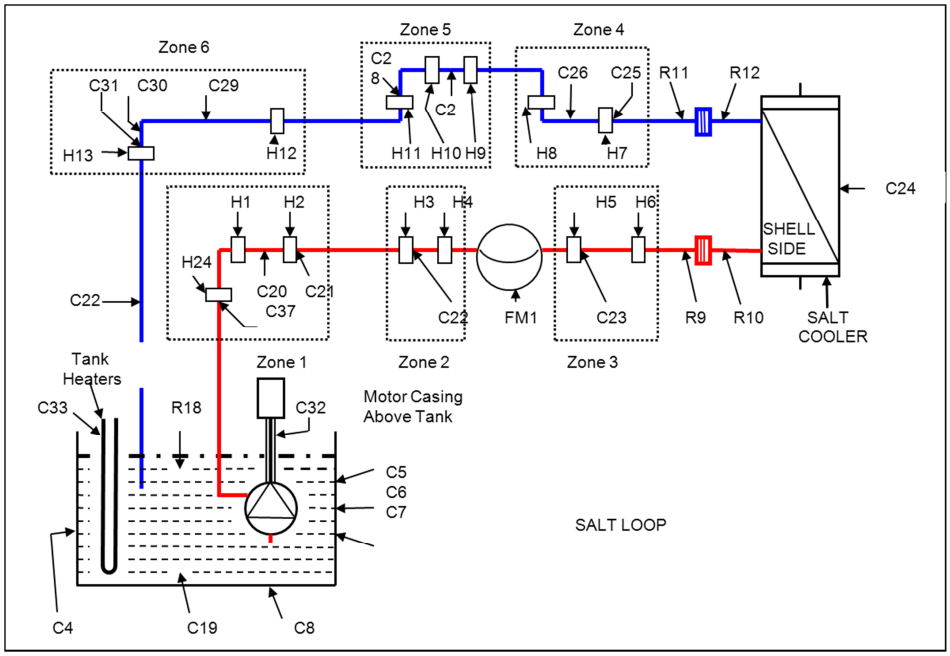

Figure 20: Salt Loop Schematic

Heat Exchanger Issues

The heat exchanger that was built per design calculations experienced many practical problems in experimentation. Tubes were initially furnace brazed into the heat exchanger, and later welded, but differential thermal expansion during the preheat process created huge thermal stresses that cracked these joints. Furthermore, melting blockages in the system can lead to huge increases in pressure, which destroyed a bellows on the system as well as causing additional failure in the heat exchanger. Because of this, a new, simpler heat exchanger was constructed to test the heat transfer properties. A CAD rendering as well as a picture of the final heat exchanger that was utilized in the system is shown in figure 21.

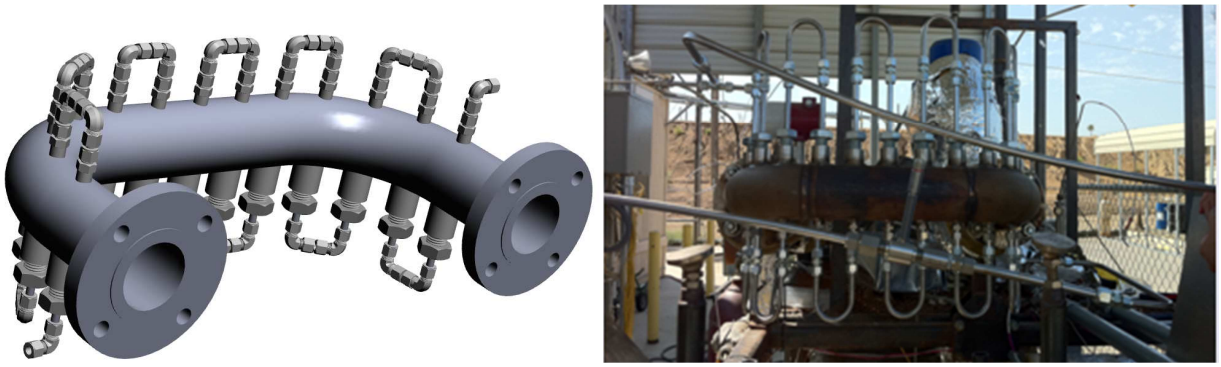

Figure 21. CAD rendering and picture of final heat exchanger utilized for experimentation.

The heat exchanger consists of a single pass on the salt side, and 13 passes on the oil side. Two RTD's were placed at both the inlet and outlet of the salt and oil in the heat exchanger. This heat exchanger design is more robust, utilizing Swagelok and valve packings to allow for more accommodation of thermal stresses. The system also allows for a much better signal to noise ratio on the oil side of the heat exchanger, allowing for better accuracy in heat transfer coefficient measurement. The heat exchanger also

has a high solid tolerance due to 84% open cross sectional area. It does suffer in terms of Reynold's number as well as maximum achievable solid fraction, but is still an excellent test bed to determine the effectiveness of the coatings utilized on the heat transfer coefficient that can be achieved.

Section 7
Experiment Results with the Laboratory Scale Prototype

Experiment Plan

- Conduct set 1 and set 2 of the planned three sets of experiments
  - Set 1 (Oil temp >salt melting point (MPt)
  - Set 2 (HX wall temp <salt MPt but salt temp > MPt)
  - Set 3 (oil temp < salt MPt and salt Temp at MPt)

Study Parameters	
Temperature of oil	various
Temperature of salt	high, medium, low
Flow rate of salt	high, low
Flow Rate of Oil	high, medium, low

Expected Outputs

Heat transfer coefficient (Ufreezesalt) as a function ofsolidification at near solification temperature
Heat transfer coefficient (Ufreezesalt) as a function of salt flow and heat transfer temperature difference
Heat transfer coeffieicent correlation from liquid molten salt
Pumpability of freezing mixture
Experience with handling high temperature molten salts near freezing point

Results of Experiments

Melting of Salt

Experiments were conducted through all three sets of proposed experiments successfully. Figure 31 shows the heat exchanger outlet salt temperature vs. the elapsed experiment time. Experiments began with an initial salt temperature of ~345 C and slowly decreased to ~302 C as the heat was extracted from the salt by the oil system (heat was utilized to help slow this process). Figure 32 shows the salt flow rate vs. the elapsed experiment time. The flow rate was modulated between 50 and 230 gallons per minute of flow rate in order to investigate the dependence of the heat transfer coefficient on the fluid velocity and reynold's number. Figure 33 shows the oil flow rate vs. elapsed experiment time. The oil flow was modulated from .6 to 1.4 gallons per minute to help determine the dependence of the overall heat transfer coefficient on the internal oil convection coefficient. Figure 34 shows the oil heat rate vs. elapsed experiment time. This varies from about 5 kW down to about 1kW as the oil and salt flow rates are varied, as well as the fact that the ΔT between the salt and oil decreases as the experiment goes on. Figure 35 shows the percent solid salt in salt tank vs. the elapsed experiment

time and figure 36 shows the percent solid salt in salt tank vs. temperature. This was calculated by a tank heat balance between heat gained from heaters and losses to the heat exchanger and environment.

Output	Oil Temperature, C (320C, 311,280,270,260, 250)	Oil Flow Rate, high=20gpm, medium=15 gpm, low=10 gpm	Salt temperature above freeze point (high=40C, med=20C, low=1C)	Salt Flow rate (high=40gpm, low=20 gpm)
liq to liq heat transfer coeff	320	high	high	high
liq to liq heat transfer coeff	320	medium	high	high
liq to liq heat transfer coeff	320	low	high	high
liq to liq heat transfer coeff	320	medium	high	low
liq to liq heat transfer coeff	311	low	high	low
solidification heat transfer coeff	311	medium	medium	low
solidification heat transfer coeff	305	medium	medium	low
solidification heat transfer coeff	300	medium	medium	low
solidification heat transfer coeff	280	medium	medium	low
solidification heat transfer coeff	270	medium	medium	low
solidification heat transfer coeff	260	medium	medium	low
solidification heat transfer coeff	260	medium	low	low
solidification heat transfer coeff	250	medium	low	high
solidification heat transfer coeff	250	medium	medium	low
solidification heat transfer coeff	320	medium	high	low
shut down mode	320	medium	heaters off	pump off
shut down mode	fan on	pump off	heaters off	pump off

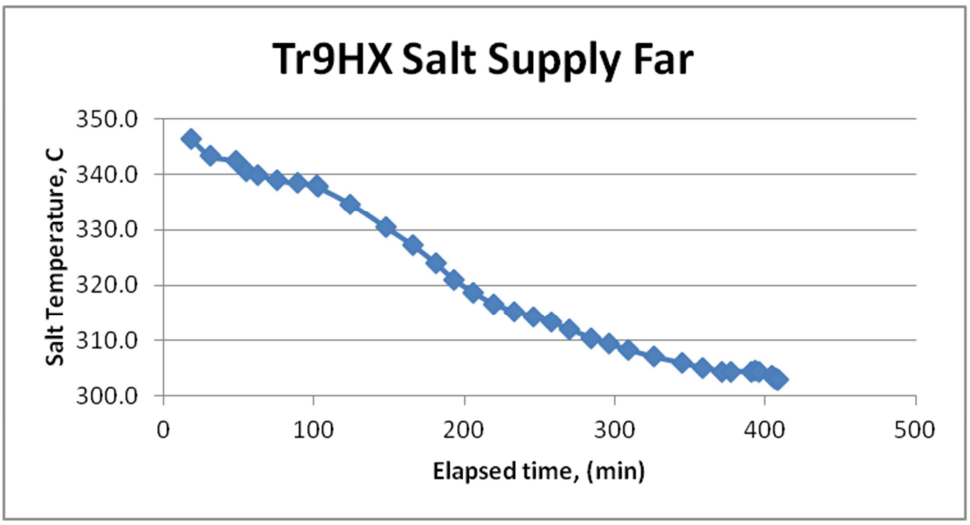

Figure 31: Heat Exchanger Outlet Salt Temperature vs. Elapsed Experiment Time

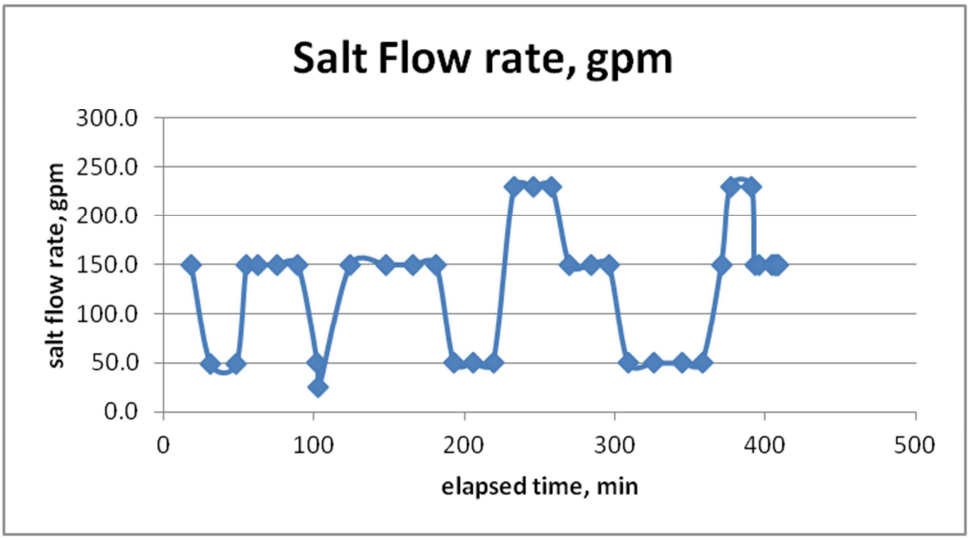

Figure 32: Salt Flow Rate vs. Elapsed Experiment Time

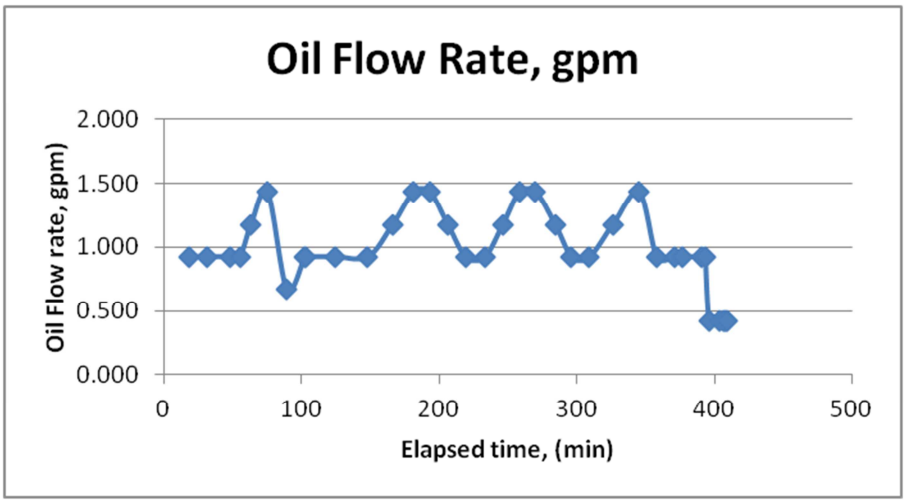

Figure 33: Oil Flow Rate vs. Elapsed Experiment Time

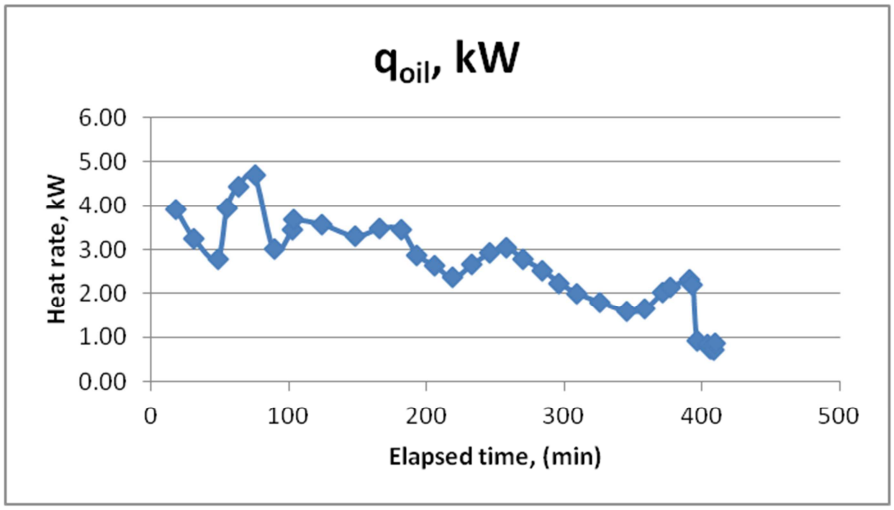

Figure 34: Oil Heat Rate vs. Elapsed Experiment Time

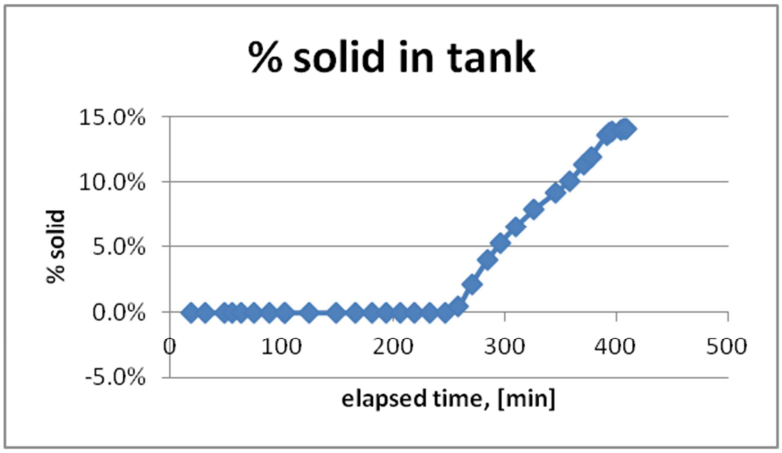

Figure 35: Percent Solid Salt in Salt Tank vs. Elapsed Experiment Time

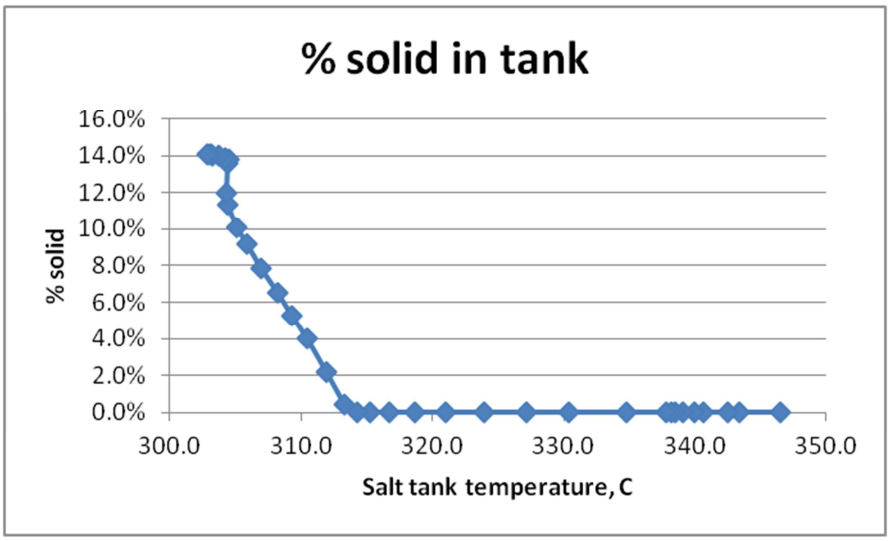

Figure 36: Percent Solid Salt in Salt Tank vs. Salt Temperature

Figure 37 shows the overall heat transfer coefficient, U, vs. salt temperature. It ranges from values as high as 2400 W/m^2K above the melting point at high salt flow rates, to around 500 W/m^2 K at the salt melting point. Figure 38 shows the predicted salt thickness on the heat exchanger tubes vs. temperature. This was calculated utilizing the math model to be presented later, but is a calculated measure of how thick the salt layer on the surface should be to produce a given heat transfer coefficient. Using this, the salt thickness on the tubes was calculated for the given heat transfer properties from the experimental data. Figure 39 shows the calculated salt thickness on the heat exchanger tubes vs. temperature and figure 40 shows shows the calculated salt thickness on the heat exchanger tubes vs. elapsed experiment time. This data can be summarized in figures 41 and 42. Figure 41 shows the overall heat transfer coefficient vs. temperature at different salt flow rates. We can see that for temperatures above the melting point (~308-310^{o}C) we achieve very high heat transfer rates around ~1600 W/m^2 K. This number drops

dramatically as we near the solidification temperature (~303 ^{o}C) to ~1050 W/m^2 K. Figure 42 shows the overall heat transfer coefficient vs. salt flow rate at different temperatures. This graph shows that the heat transfer coefficient is relatively unaffected by flow rate at these low Reynold's numbers, and is dominated more by temperature.

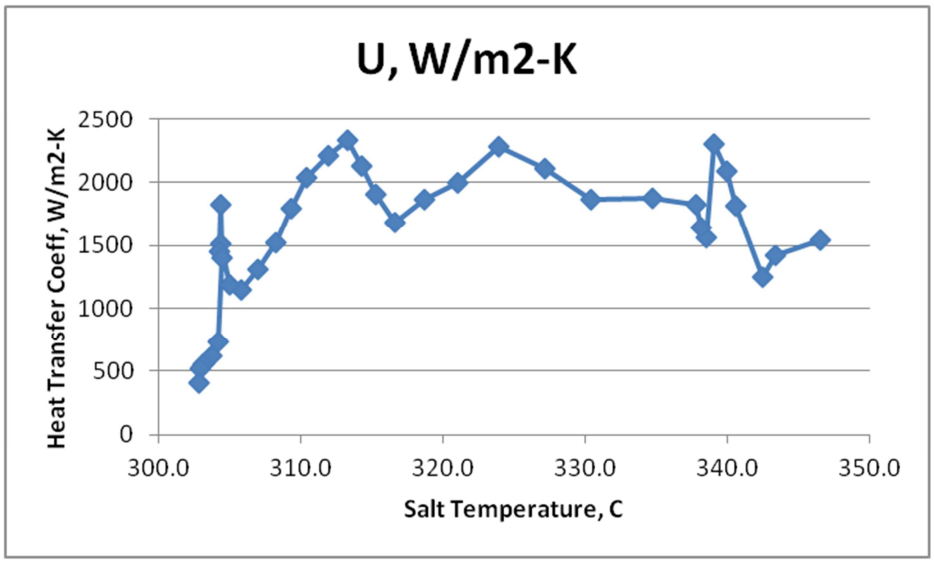

Figure 37: Overall Heat Transfer Coefficient vs. Salt Temperature

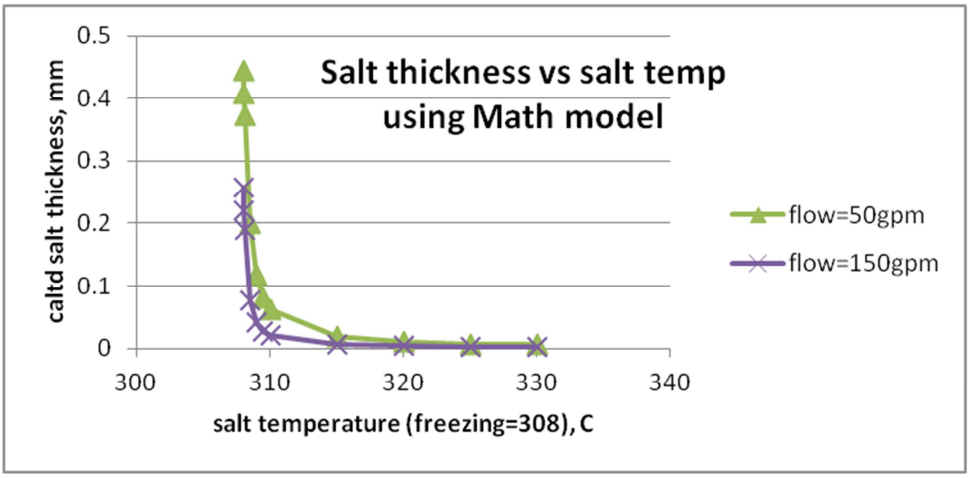

Figure 38: Calculated Salt Thickness vs. Salt Temperature by Math Model

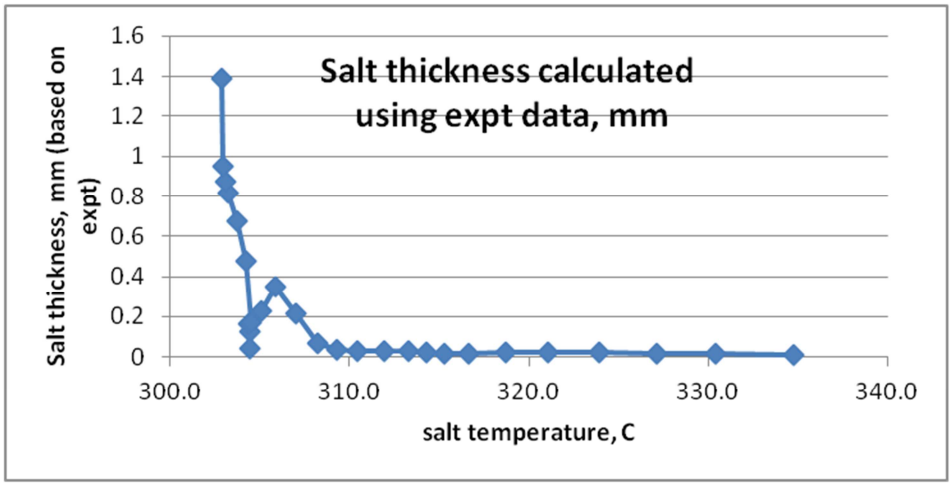

Figure 38: Calculated Salt Thickness vs. Salt Temperature by Experimental Data

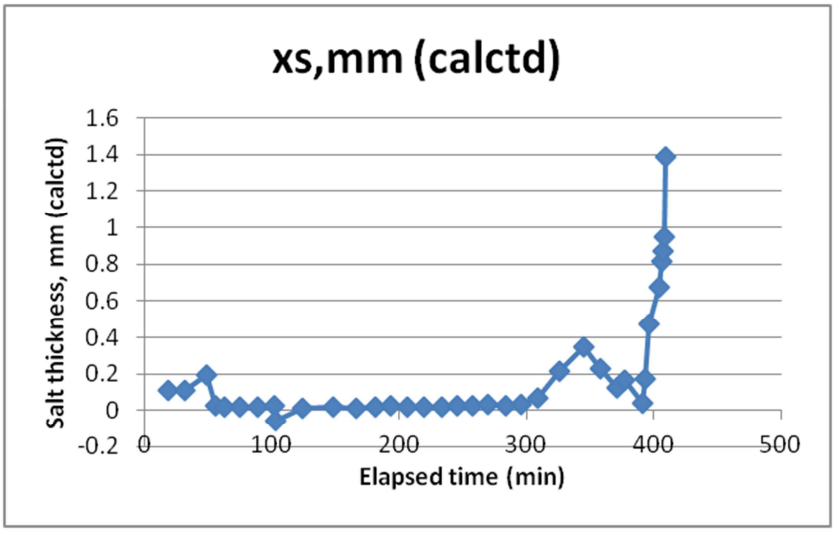

Figure 40: Calculated Salt Thickness vs. Elapsed Experiment Time

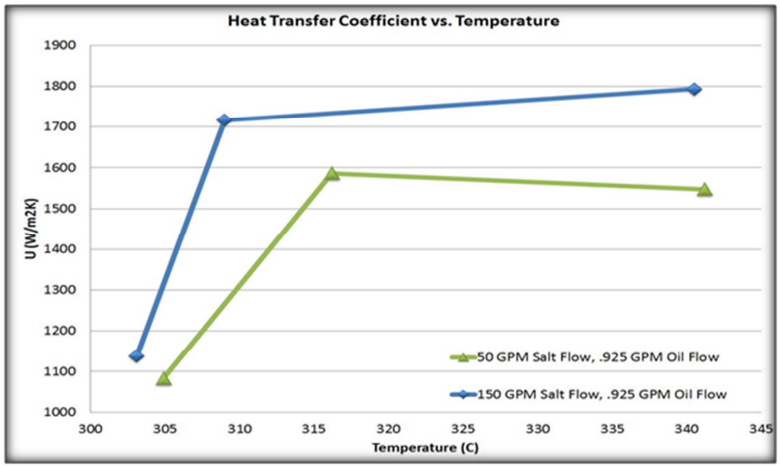

Figure 41: Overall Heat Transfer Coefficient vs. Temperature at Different Flow Rates

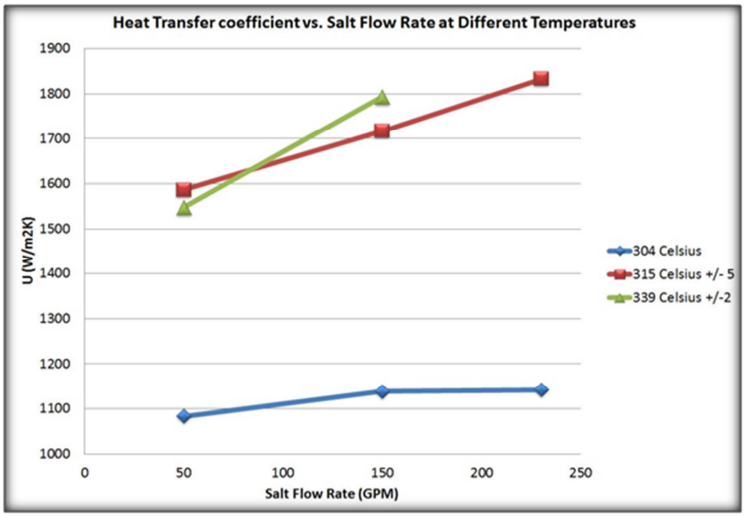

Figure 42: Overall Heat Transfer Coefficient vs. Salt Flow Rate at Different Temperatures

Section 8.
Economic Analysis of PCM-TES with CSP

The LCOE objective can be achieved by the following three factors:

- Technical Improvements from efficient and optimized systems
- Economy of Scale cost reduction due to increased size
- Volume Production discounts resulting from construction of multiple plants, or from procurement of multiple subcomponent parts.

The primary reduction in LCOE of this project will be due to the first bullet: technical improvement resulting from reduced use of salt, smaller container size and from improved turbine efficiency.

Figure 8-1 illustrates the impact of heat of fusion and salt costs on total TES cost. The total TES cost is sum of capacity cost and rate-related costs. The TES cost shown in Figure 8-1 is relative cost and is based on assumed data on costs of heat exchangers, tank and balance of plant.

Capacity Costs ~ 1/Heat of fusion of salt

Rate-Related Cost ~ $1/\sqrt{\ }$ (Thermal conductivity X Heat of Fusion)

The capacity-related costs are inversely proportional to the heat of fusion while the rate-related costs depends on the heat exchanger area required and is inversely proportional to the square root of heat of fusion multiplied by the thermal conductivity of the selected salt.

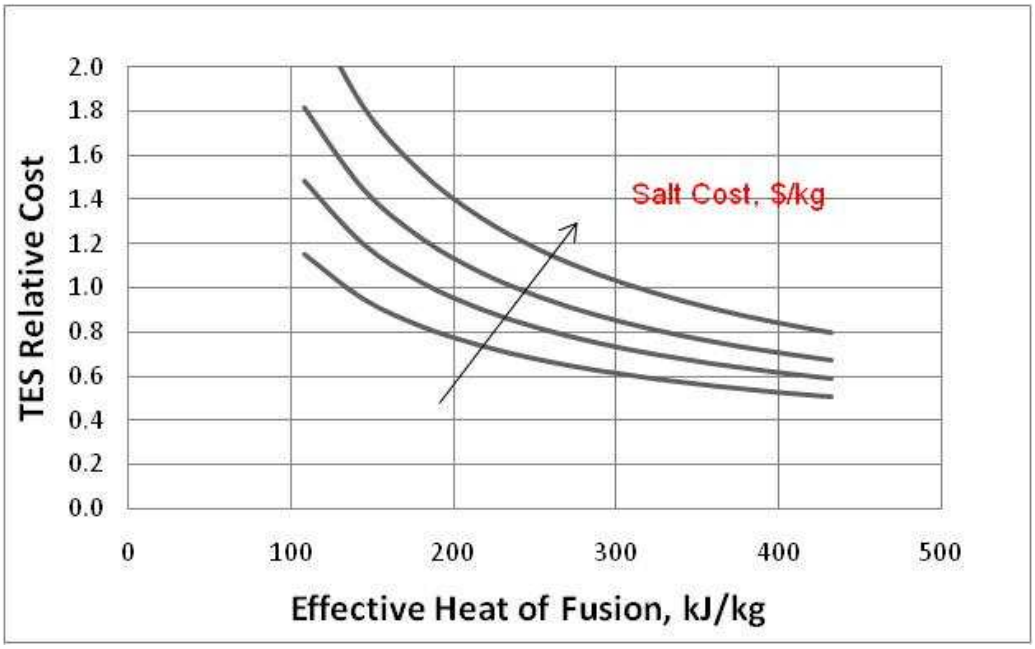

Figure 8-1

The economic analysis uses a nitrate as the baseline salt for calculations.

Benefits of active heat exchange PCM TES

When compared to a two-tank conventional sensible heat TES, the PCM –TES:

- Reduces the amount of salt required by 8% for a 6 hour storage
- Improves CSP plant system efficiency by 0.9% because TES can be charged with lower receiver temperature (450^{o}C instead of 550^{o}C) during periods of low solar flux. The heat is used to melt the salt and bypass the high temperature heat exchanger (see figure 8-2)
    - Simulations using power tower model (PWR) calculate an overall improvement in annual system efficiency of 0.88% or a reduction of 0.88% in system cost for same annual energy. Since TES costs are 10% of the system cost, this represents 8.8% reduction in equivalent costs assignable to TES.
- Uses a single container with actively managed thermal stratification to provide for superheat and vaporization of water. This eliminates the need for the lower cost carbon steel tank.

Additional costs of active heat exchange TES

- Custom design of heat exchanger using coated tubes.
- Additional molten salt pump to pump fluid from storage tank through the high temperature heat exchanger during charge
- Additional charge cycle heat exchanger to transfer heat from receiver heat transfer fluid to storage fluid.

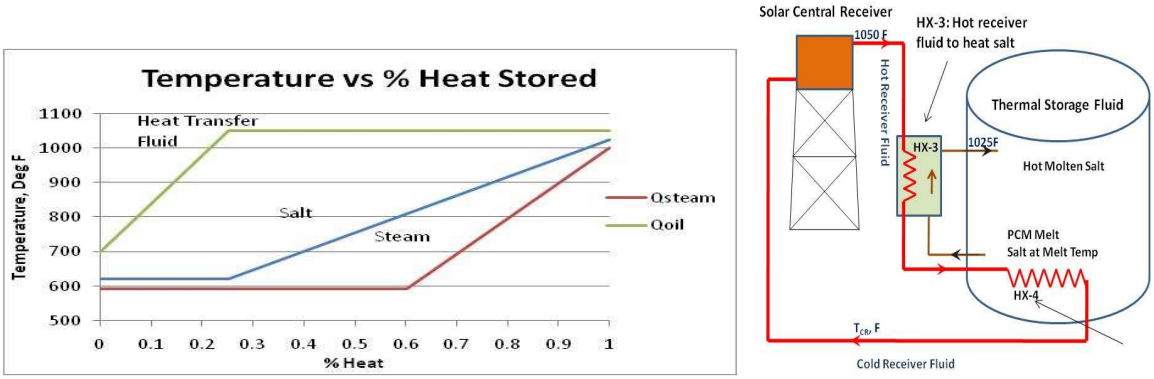

Figure 8-2. Heat transfer fluid temperature for charging TES need not be constant

Table 8-1 shows the estimates of dollar savings with the active heat exchange PCM-TES when compared to a two-tank sensible heat exchange system for two different solidification percentages (even though we used absolute costs, the table should be used for comparing costs between systems). Our goal was to achieve 40% solidification. However, we project we can achieve15%. The table shows costs for both these cases.The conventional sensible heat storage system is a two-tank TES using molten salt as heat transfer and storage fluid, storing heat between 550 ^{o}C and 330 ^{o}C. The heat exchangers are sized to provide heat rate to generate100MWe during discharge. The additional cost due to lower heat transfer coefficient and special coating for the steam generating power block heat exchangers, is included in the PCM-TES columns. The cost of the heat exchanger is assumed to be 25% more for PCM-TES than the nominal cost for a shell and tube heat exchanger in 2-Tank system. Also, PCM-TES system requires

additional heat tracing on piping to and from the heat exchangers, which is assumed to be 5% of the total cost of the system.

The TES cost savings with 15% solidification is 9% whereas for 40% solidification, the net benefit can be up to 21%. However, including the credit for improved system efficiency assignable to PCM-TES the expected savings are 30% and 17% over the two-tank TES for the 40% and 15% solidification respectively.

Even though, we demonstrated that solidifying *a dilute eutectic over coated tubes* can improve heat transfer and reduce the amount of salt used, the savings for the 15% solidification PCM-TES are at best marginal. This is because there are uncertainties in the additional parasitic energy for pumping the high viscosity salt slurry and parasitic energy for additional heat tracing which will increase the operational cost.

Table 8-1 Comparison of Benefits and Costs with PCM-TES and 2- Tank Sensible TES

Solidification %	%		0%	40%	15%
	$/kWht		**$ 28.20**	**$ 22.35**	**$ 25.79**
			2-Tank Sensible 287C to 550C	**1- Tank Active HX TES 300 C to 550C**	**1- Tank Active HX TES 300 C to 550 C**
			263	**250**	**250**
Qsto	MWHt		2000	2000	2000
Delta T	deg F		473.4	450	450
Latent Heat	Btu/lb		0	34	12.75
% volume solid	%		0%	0%	0%
% available volume	%		90%	95%	95%
Specific heat	Btu/ft3/F		45.6	45.6	45.6
Specific heat	Btu/lb/F		0.380	0.380	0.380
Specific store capacity	Btu/ft3		19428	23574	21024
Specific store capacity	Btu/lb		161.9	194.8	174.6
Effective Specific heat	Btu/lb/F		0.34	0.43	0.39
Lbs of Media	lbs		42,148,746	35,039,795	39,092,016
Vol of Media	ft3		351,240	289,471	324,581
No. of tanks			2	1	1
H/D			0.5	0.5	0.5
Diameter (Max=150)	ft		76	94	99
Height (Max=42)	ft		38	42	42
Foundation area	ft2		9107	6892	7728
Surface area	ft2		18213	19253	20817
Pressure at tank bottom	psi		32	35	35
thickness avg	ft		0.334	0.382	0.393
2 tank or 1 tank cost factor (1 for SS tank, 1.65 for SS+Carbon steel tank	est		1.65	1	1
Lbs of steel	lbs		8,034,791	3,996,485	4,485,876
Learning factor			0.81	0.81	0.81
Storage Tank cost			$ 16,968,323	$ 8,440,002	$ 9,473,526

Insulation Cost	$/ft2	30	$ 546,403	$ 577,577	$ 624,500
Surge Tanks	% of tank	3%	$ 509,050	$ 253,200	$ 284,206
Foundation costs	$/ft2	350	$ 3,187,351	$ 2,412,262	$ 2,704,845
Pumps	est	25%	$ 4,242,081	$ 4,242,081	$ 4,242,081
Interconnection pipes		10%	$ 1,696,832	$ 844,000	$ 947,353
Instrumentation & Controls		2%	$ 543,001	$ 335,382	$ 365,530
Total	$		$ 27,693,041	$ 17,104,505	$ 18,642,040
Coated tube HX, Additional charge HX	est		-	$ 3,600,000	$ 6,100,000
Salt	$/lb	$ 0.53	$ 22,338,835	$ 18,410,384	$ 20,643,379
Other Misc (Contingency)	% total	5%	$ 1,384,652	$ 855,225	$ 932,102
additional for heat tracing	5% total	5%	$ -	$ 855,225	$ 932,102
Direct Total			**$ 51,416,528**	**$ 40,825,340**	**$ 47,249,623**
Indirect					
Sales Tax (8.75% on material)		8.75%	$ 3,447,632	$ 2,644,895	$ 2,918,162
Engineering - (3% of direct)		3%	$ 1,542,496	$ 1,224,760	$ 1,417,489
Total Cost of TES			**$ 56,406,656**	**$ 44,694,995**	**$ 51,585,274**
Specific Costs	$/kWht		$ 28.20	$ 22.35	$ 25.79
Relative Cost			100%	79%	91%
Savings				**21%**	**9%**
0.88% improvement in System Efficiency credit for lower temp charging				8.80%	8.80%
Expected Total Savings				29.6%	17.3%

Section 9.
Lessons Learned
Design Considerations for Molten Salt Thermal Storage

Several lessons were learnt in the design, building and operating of the two flow loop systems. The fact that these systems were operating close to the salt freezing point presented some foreseen and unforeseen challenges.

Lessons learnt from Phase 1 Flow Loop:

- First melt of salt in granular form versus subsequent melts when it is a solid mass have to be handled entirely differently. The first time melt needs to be managed to account for inefficient heat transfer from heating surfaces to salt, extra heating time as a result and gradual charging of salt to avoid air pockets and ensure homogeneous molten liquid formation.
- Once the required quantity of salt is melted, it is very important to keep the salt in the molten state for the longest duration possible, preferably until the series of experiments is completed, so as to avoid the complications mentioned below.
- Subsequent melts have to be handled with extreme care. When frozen salt in a tank and pipes is required to be melted, the process of melting needs to start from the salt surfaces exposed to the atmosphere. In other words, the surface of the salt should be melted first and proceeding gradually to the inside. Due to practical considerations of heater placement this is not always possible. Typically heaters are attached to the surface of the tank and pipes and heating starts at those surfaces. As the salt melts at these surfaces its volume expands and pressure pockets are created leading to explosions. There were two such blowouts in the Phase 1 Flow Loop. Safety precautions prevented any damage to property or personnel.
- In the event that it becomes necessary to shut down the flow loop prior to the completion of experiments, a salt drainage system is necessary that can quickly drain the molten salt from the system prior to shut down.
- It is important to drain all pipes and fittings of molten salt after each experiment to prevent solidification. Any solid salt formation in pipes and fittings presents serious challenges to safe re-melting.

Lessons learnt from Phase 2 Flow Loop:

- Salt Melting System for first time melting of salt should be designed to ensure easy flow of melted salt into the molten salt tank. The entire salt flow path should be adequately heated to prevent any freeze ups. The heating system should be designed for maximum hot surface area to be in contact with salt. Heaters should be chosen to ensure best possible contact with the pre-melt tank and be able to withstand hot spots that develop.
- Heat exchangers and all other salt flow paths should be designed to safely withstand the maximum system pressures that might develop in case of freeze ups in the salt flow path.
- Since the salt flow path is designed to automatically drain the salt into the tank at the end of each experiment, there may be a possibility of air locks building up. A suitable vent system should be in place to take care of such a possibility.

- Immersion Heaters are preferred over tank surface heaters.
- Heater placement should be designed for easy replacement in case of failures.
- The system should be designed to keep the salt molten for the entire duration of operation.
- In case of unscheduled system shut downs, salt may freeze and it may become necessary to re-melt the frozen salt in the tank. To facilitate re-melting, immersion heaters should be placed so as to heat the salt so that the salt at the top melts first. This will prevent excessive pressure build-ups.
- Care should be taken to ensure that temperatures of heater surfaces not immersed in salt do not exceed safe levels and also levels that might decompose salt.
- Significant conduction losses occur through the body of the salt pump and the discharge and return pipes. Sufficient trace heating should be provided as close to salt level as safely possible to account for such heat losses and prevent freeze ups.
- Temperatures of salt should be monitored in as many locations in the tank as possible.
- A stirring should be considered for periodic slow stirring of salt in the tank to ensure uniform temperature.
- All piping should be adequately heat traced. This is extremely important if pipes with a low thermal conductivity material such as stainless steel are used.
- Temperatures of the entire salt flow path should be monitored at as many points as possible.
- Prior to starting the salt flow, every time, the salt flow path should be checked to ensure that there are no freeze ups or blockages. This can be done with a simple pressure test using air.
- Emergency procedures to shutdown the system should be in place. A *single emergency shutdown* actuator (button) that will simultaneously shutoff pumps, close or open relevant valves, turn on or off heaters etc should be provided at multiple locations in the plant.
- Salt re-melt procedures in case of unforeseen shut downs should be in place. Due consideration should be given to salt melt process so that it melts from the top and no pressure pockets are formed inside the frozen salt block.
- Safety procedures for operation of the system should be in place. All system conditions should be foreseen and accounted for to the extent possible. A thorough Failure Mode Effect Analysis (FMEA) must be conducted with all operating personnel in attendance.